ALMA MATER STUDIORUM – UNIVERSITÀ DEGLI STUDI DI BOLOGNA

Facoltà di ingegneria

Dipartimento di ingegneria dell'energia elettrica e dell'informazione

Master degree in Telecommunications Engineering

TESI MAGISTRALE

in

Antennas for Wireless Systems

FREQUENCY-DIVERSE ARRAYS DESIGN FOR ACCURATE WIRELESS POWER TRANSMISSION

Candidato	*Relatore:*
Enrico Fazzini	*Prof. Ing. Diego Masotti*

Correlatori:

Chiar.ma Prof. Ing. Alessandra Costanzo

Ing. Mazen Al Shanawani

Anno Accademico 2019/2020

Prima sessione

1

Sommario

1. INTRODUCTION

"Wireless power transfer (WPT), wireless power transmission, wireless energy transmission (WET), or electromagnetic power transfer is the transmission of electrical energy without wires as a physical link. In a wireless power transmission system, a transmitter device, driven by electric power from a power source, generates a time-varying electromagnetic field, which transmits power across space to a receiver device, which extracts power from the field and supplies it to an electrical load. The technology of wireless power transmission can eliminate the use of the wires and batteries, thus increasing the mobility, convenience, and safety of an electronic device for all users. Wireless power transfer is useful to power electrical devices where interconnecting wires are inconvenient, hazardous, or are not possible. "[1]

Since Tesla and Marconi discovered the use of electromagnetic field for transmitting energy and information respectively, the human being has always had interest in developing this technology. This interest has led us into the industry revolutions and now we find ourselves immersed in what is called the "industry 4.0".

In this scenario a prestigious position is kept by the WPT technologies. The reason of interest on this application is related to the fact that this revolution, led at the moment by the 5G, will require in a near future billions of devices interconnected one to each other. The necessity to charge them is one of the hot topics and, since the use of the wires is slowly disappearing for obvious reasons, the WPT technology results the only method able to support this technological revolution. As a consequence several ICT companies have moved their interests to this new research field increasing the WPT market value during the years, as shown in the following figure:
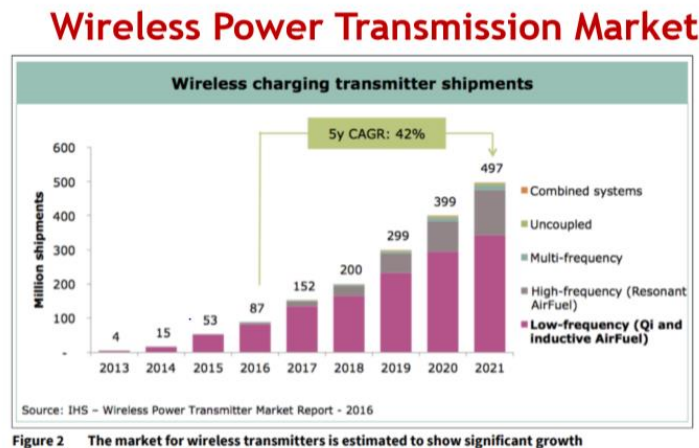

Figure 1.1 – Wireless Power Transfer market, [2]

Inside the WPT scenario a classification is needed based on the properties of the electromagnetic field. Considering the following scheme:

Figure 1.2 – Classification of WPT technologies, [2]

Based on where the interaction between transmitter and receiver happens, we can divide:

- NEAR FIELD NON RADIATIVE WPT

  - It is usually implemented by the exchange of magnetic flux between two coils
  - It can have strong or loose coupling
  - It can be resonanant or non resonant
  - It involves high level of power

- FAR FIELD RADIATIVE WPT

  - It is usually implemented using the radiative electromagnetic far-field between radiating elements
  - It can cover long distances
  - It typically involves low level of power

The detailed properties of both are listed in the following figure:

Wireless energy transmission

	NF–WPT		FF–WPT
	Resonant	Non–resonant	
TX mechanism	Coupling, no wave propagation	Coupling, no wave propagation	Wave propagation
Interacting device	Coils/electrodes	Coils/electrodes	Antennas
TX–RX interaction	Strong interaction	Medium interaction	No interaction
Operating frequency	LF, HF	LF, HF	Microwave, millimeter–wave
Power level	Medium (mW–W), High (kW)	Medium (mW–W), High (kW)	Ultra–low (μW–mW) High (MW)
Efficiency	High (70–90%)	Medium (30–60%)	Low (10–50%)
Commercial applications	Yes	Yes	No

Figure 1.3 – Properties of WPT near field and far field, [2]

Whatever the involved technology the most important figure of merit in any WPT scenario is the efficiency:

WPT: it is a matter of efficiency

$$\eta_{LINK} = \eta_{DC-TF} \cdot \eta_{TF-TF} \cdot \eta_{TF-DC} = \frac{P_{TX}}{P_{BIAS}} \cdot \frac{P_{RX}}{P_{TX}} \cdot \frac{P_{DC}}{P_{RX}}$$
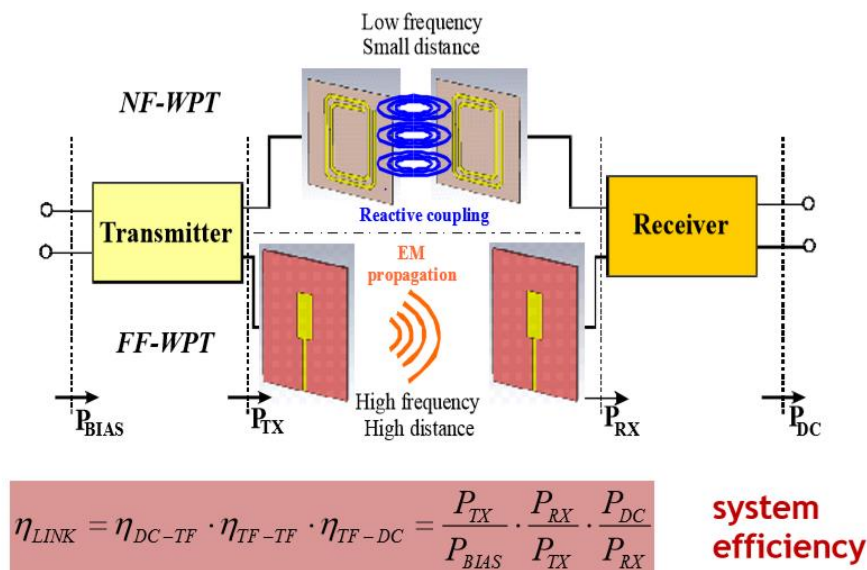
system efficiency

Figure 1.4 – WPT efficiency, [2]

As it is possible to notice the efficiency of the entire link is given by the product of three main contributes:

- The starting efficiency related to the conversion from DC to RF
- The efficiency related to the wireless link (from RF to RF)
- The final efficiency related to the conversion from RF to DC

The main interest of this thesis job is on the far-field WPT applications. In the recent years, many research efforts have been made to make the far-field wireless power transfer (WPT) feasible. The research activity has followed three main directions in order to maximize the overall wireless link efficiency: i) the optimization of the power amplifier dc-to-RF efficiency on the transmitter side; ii) the optimization of the RF-to-dc efficiency of the receiving rectifying antenna (or rectenna); iii) the study of smart transmitting architecture for the maximization of the RF-to-RF link efficiency. As regards the first two research directions, one can say that results very close to the optimum have been already achieved: over 80% drain efficiency amplifiers are available in the microwave range, as well as highly efficient rectennas (with RF-to-dc efficiency greater than 60%) working in the -10 dBm ÷ 10 dBm RF available power range, typical of WPT applications, can be considered a reality. A great deal of activity has been also devoted to the third branch, but this can be considered the main bottleneck in far-field WPT: the envisaged exploitation of millimeter waves in future 5G networks also for powering purposes will be possible only if transmitting systems will reach a high level of reconfiguration in real time, together with the more demanding power focusing capability.

This thesis work is born with the intent of researching an implementation for the increase of the RF-to-RF efficiency with a new emerging technology called FREQUENCY DIVERSE ARRAY (FDA). This work started in september 2019 and had a duration of about 10 months, until July 2020. During this period, the research activity was split mainly in three parts:

1) From September 2019 to December 2019 the FDA systems have been studied, in particular the use of frequency diversity among array elements in order to focus the beam in a specific region of the space, i.e. the use of slightly different radiating frequency of the antenna elements that offers a range dependent radiation mechanism. Starting from the classical configuration of FDA, other more complex structures have been studied, with particular emphasis on the Frequency Diverse Array with logarithmic frequency distribution. After this preliminary study, a mathematical evaluation of the radiating mechanism under investigation has been provided and numerical simulations with MATLAB have been performed.

2) From December 2019 to January 2020 the design of the front-end under investigation has been performed, with the use of electromagnetic and circuital (through Harmonic Balance technique) simulators. A successful agreement between the results of the linear numerical simulation provided in the first period and the more accurate nonlinear/electromagnetic simulation of this phase has been achieved.

3) Finally form February 2020 and July 2020 an overall FDA system set-up has been investigated from the realization point of view. From the starting point, in September 2019, the most important question on FDA was related to how to control these complex radiating systems with the technology available on the market. A solution has been found and identified with the emerging Software Defined Radio (SDR) technology. Therefore this last period has been dedicated to the comprehension and characterization of the SDR platform Zynq Ultrascale+ ZCU111 Evaluation Kit. The period spent on it has requested the study of several concepts of digital processing and, towards the end of June, the characterization of the board and the comprehension of the tools used to control it have been deeply studied.

The entire work done on this new topic has provided an improvement with respect to the state of art. In fact, until now neither circuit-based simulations of such a complex radiating system nor practical implementations of FREQUENCY DIVERSE ARRAY were proposed, especially with the use of the SDR technology. These innovative steps forward have led to the acceptance for the presentation of two papers [5, 6] in two of the most important conferences on WPT: the Wireless Power Transfer Conference-WPTC (within the Wireless Power Week 2020) [5] and the European Microwave Week-EUMW 2020 [6]. The presentation of the first one at the WPTC should have been at the end of May, but has been postponed to November because of the Corona virus situation. The second one will be presented in January 2021. The innovative idea behind these works has been and is currently exploited by the University of Bologna unit within the framework of the

National project PRIN2017-WPT4WID (Wireless Power Transfer for Wearable and Implantable Devices), with the aim of proposing new strategies for accurate wireless power transfer in the millimeter wave spectrum.

After this introduction, in the second chapter the analytical evaluation of different FDA systems radiation mechanism is proposed, starting from the innovative array factor of whatever kind of FDA and proceeding to the classification of the radiating systems under investigation. With the use of MATLAB a script evaluating the different configurations has been developed and the results of this linear numerical simulation is provided. Particular emphasis is given to the FDA family with a logarithmic distribution of the frequency among the antennas with, at the end of the chapter, a first practical approach to the design of such a kind of system, with the description of some practical problems to be faced.

In the third chapter, the more accurate electromagnetic (EM) and circuital co-simulation results will be provided. The simulations were performed with the CST software tool (for the EM calculations) and the nonlinear (NL) circuit Simulator based on the Harmonic Balance technique developed by the electromagnetic field lab staff of the DEI. First, the single planar monopole antenna and its combination in an 8-element array has been electromagnetically designed; then, the corresponding results have been extracted and inserted into the NL simulator for the rigorous nonlinear/electromagnetic co-simulation of the selected FDA system, with the logarithmic distribution of the frequency. The corresponding encouraging results have been compared with the linear ones and will be described in detail in this chapter.

In the fourth chapter, the emerging technology of Software Defined Radio is presented through the explanation of the Zynq Ultrascale+ ZCU111 Evaluation Kit. A first theoretical approach is given with the introduction of some basis concepts useful to understand the passage from analog to digital domain. Then two tests are presented: the loopback test and the RF characterization of the board. The first one is able to show the power of the graphical tools of thee adopted SDR able to manage the data converter subsystem, called RF Data Converter Evaluation Tool: he main blocks functionalities offered by the platform can be understood in this part of the chapter. The second test is used to show the RF characteristics of the output spectrum with one- tone and two-tone analysis examples.

In the fifth and final chapter a complete system view is offered, introducing the final implementation of the FDA with logarithmic distribution of the frequency with the explanation of the board components able to allow the control of all the 8 channels of the ZCU111. The final conclusions are then presented with some improvements to be adopted to face the problems met during this thesis job.

2. FREQUENCY DIVERSE ARRAY SYSTEMS

In this section the frequency diverse array denominated here FDA will be introduced, and it will be provided the analytical formulation for the description of the behaviour of this new array concept. The starting point will be the presentation of analytical calculation of the array factor. Here will be provided a new method in order to obtain it, different from the canonical one that makes use of radiating vectors, starting from the set of transmitted signals.

Next it will be provided a theoretical classification of the FDA's scheme, highlighting the strengths and defects of the several configurations, with particular emphasis on the frequency diverse array with logarithmic increasing frequency offset.

The several configurations have been analyzed with the use of several scripts in MATLAB that provide the array factor and the beam pattern properties. They will be presented in the following sections.

2.1 ANALYTICAL FORMULATION OF THE ARRAY FACTOR

It is considered the following system, showed in the figure 2.1, composed by:

- M radiating elements
- The element with index "0" will be considered as "element zero" and it will be centered in the origin of xy system reference
- Every element has a distance d_m respect to the element zero
- Every element radiates at frequency f_m computed with respect to the operating frequency of the zero element f_0
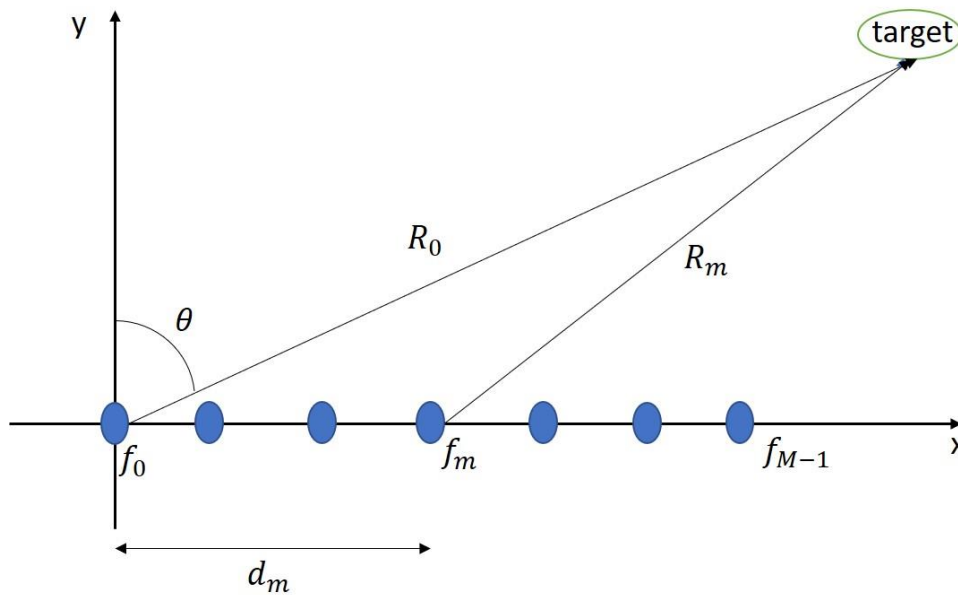- The target has a distance R_m from the m_{th} element

Figure 2.1.1 - Asymmetric Array System

The parameters d_m and f_m can be expressed as function of the element zero's quantities:

$$d_m = d_0 * \Delta d_m \qquad where \ d_0 = \frac{0.5f_0}{c}$$

$$f_m = f_0 + \Delta f_m \qquad where \ f_0 = frequency \ of \ the \ zero \ element$$

Now the transmitted signal of the m_{th} element, denoted with $x_m(t)$ is considered:

$$x_m(t) = a_m \exp(j2\pi f_m t) \qquad where \ a_m \ is \ the \ complex \ weight \ of \ the \ m_{th} \ element$$

For the sake of simplicity, the phase contribution has been not considered, posing it equal to zero for every element, without lossy of generality.

The signal is computed at the distance R_m in far field condition, and the total signal transmitted at the target position can be expressed as follow:

$$x(t) = \sum_{m=0}^{M-1} a_m \exp\left(j2\pi f_m \left(t - \frac{R_m}{c}\right)\right)$$

The assumption of far field condition allows to re-write the quantity R_m as:

$$R_m = R_0 - d_m \sin(\theta)$$

Therefore the expression can be tailored in the following way:

$$x(t) = \sum_{m=0}^{M-1} a_m \exp\left(j2\pi f_m \left(t - \frac{R_0 - d_m \sin(\theta)}{c}\right)\right) =$$

$$= \sum_{m=0}^{M-1} a_m \exp\left(j2\pi(f_0 + \Delta f_m)\left(t - \frac{R_0 - d_m \sin(\theta)}{c}\right)\right) =$$

$$= \exp\left(j2\pi f_0\left(t - \frac{R_0}{c}\right)\right) * \sum_{m=0}^{M-1} a_m \exp\left(j2\pi(f_0 + \Delta f_m)\left(\frac{d_m \sin(\theta)}{c}\right)\right) * \exp\left(j2\pi\Delta f_m\left(t - \frac{R_0}{c}\right)\right)$$

It can be noticed that the first factor, the only one $m\_$independent, represents the contribution of the element zero at the target position. The second factor represents the array factor as function of:

- The frequency difference with respect to the element zero's operating frequency
- The distance of m_{th} radiating element with respect to the element zero

It can be noticed that generally speaking the following property can be assumed:

$$f_0 \gg \max(\Delta f_m)$$

Therefore, exploiting the previous relationship and replacing in the formulation the value of r with that one of R_0, the following general formulation can be reached:

$$x(t) = \exp\left(j2\pi f_0 \left(t - \frac{r}{c}\right)\right) * \sum_{m=0}^{M-1} a_m \exp\left(j2\pi f_0 \left(\frac{d_m \sin(\theta)}{c}\right)\right) * \exp\left(j2\pi \Delta f_m \left(t - \frac{r}{c}\right)\right)$$

The array factor can be written as:

$$AF(t,\theta,r) = \sum_{m=0}^{M-1} a_m \exp\left(j2\pi f_0 \left(\frac{d_m \sin(\theta)}{c}\right)\right) * \exp\left(j2\pi \Delta f_m \left(t - \frac{r}{c}\right)\right)$$

The found expression highlights the dependency of the array factor on the time, angle and range variables.

For the sake of simplicity, the value of the complex weights a_m will be considered equal to 1 in the next formulations.

After having found an analytical formulation in order to describe the array factor, in the following sections a classification of antenna arrays will be presented.

2.2 UNIFORM PHASED ARRAY

This configuration is the classical configuration of an antennas array, for which all the elements radiate at the same frequency and are spaced of the same quantity d_0 one from each other. Even if this configuration is not object of this work, its characterization is provided in order to check the correctness of the formulation found in the previous section.

The configuration of a uniform phased array, from this point identified with UPA, leads to the following relationships:

$$f_m = f_0; \quad \Delta f_m = 0 \ \forall m$$
$$d_m = m * d_0 \quad \forall m$$

The array factor can be written as:

$$AF(\theta) = \sum_{m=0}^{M-1} \exp\left(j2\pi f_0 \left(\frac{d_m \sin(\theta)}{c}\right)\right)$$

As it is possible to note, the array factor becomes function of the sole azimuth value, and the maximum radiation is in the broadside direction (q=0°) since all the elements are excited in phase, as hypothesis. This result confirms the correctness of the previous formulation since it can be reached using the classical antenna array theory using the radiation vector formulation.

With the use of MATLAB a simulation is performed considering M = 8, $f_0 = 2{,}45\ GHz$, providing the following beampattern, defined as the module square of the Array Factor AF:

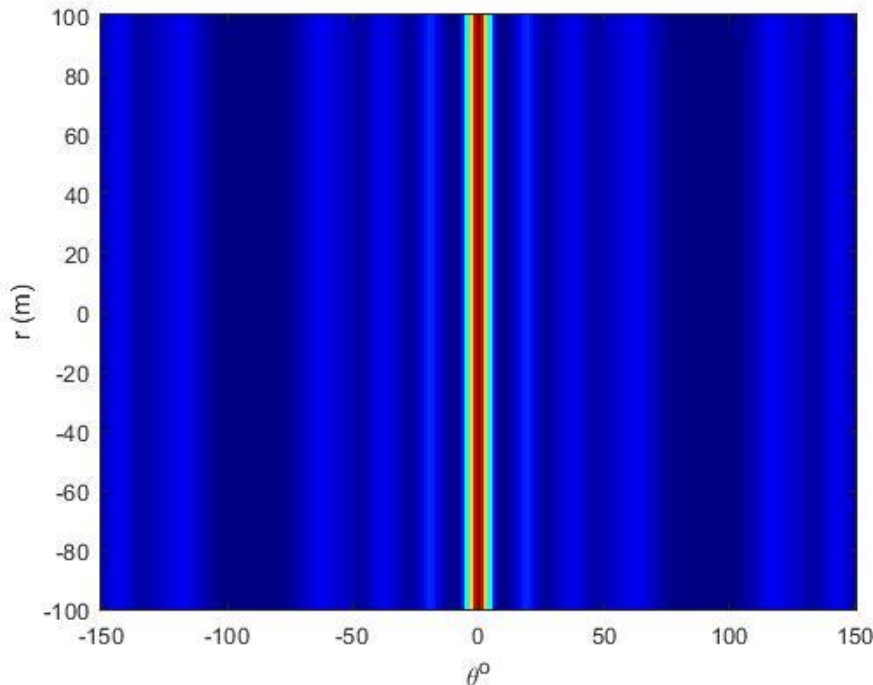$$BP(t,\theta,r) = |AF(t,\theta,r)|^2$$

Figure 2.2.1 – Beampattern of UPA over range and azimuth

As it is possible to observe, the radiation results broadside (in the 0° direction), confirming again the correctness of the formulation. It has to be noticed that this model doesn't take into account the attenuation of the field due to the free space (as per array factor or beam-pattern definition). That is why, for the different distances, in Fig. 2.2.1 we find the same value of the beampattern.

2.3. STANDARD FREQUENCY DIVERSE ARRAY

It is introduced now for the first time the frequency diverse array concept for which every element radiates at a frequency slightly different with respect to the neighbouring elements. As first the standard frequency diverse array, from here identified as sFDA, is introduced. The configuration provides M equally spaced elements with a linear increasing frequency offset. This information leads to define:

$$f_m = f_0 + m * \Delta f; \quad \Delta f_m = m * \Delta f \quad for \ m = 0, ..., M - 1$$

$$d_m = m * d_o \quad for \ m = 0, ..., M - 1$$

The array factor can be approximated by the following expression:

$$AF(t, \theta, r) = \frac{\sin(N\pi u)}{\sin(\pi u)} \ with \ u = \ \Delta f t - \frac{\Delta f r}{c} + \frac{d_0 f_0 \sin\theta}{c} + \frac{d_0 \Delta f \sin\theta}{c}$$

For the first time the array factor is a function of all the three variables: time, azimuth and range. In order to denote the benefits given by this configuration, a simulation with MATLAB with M = 8, $f_0 = 2.45 \ GHz$, $\Delta f = \ 5 \ MHz$ is provided. The results are shown in the following figure:
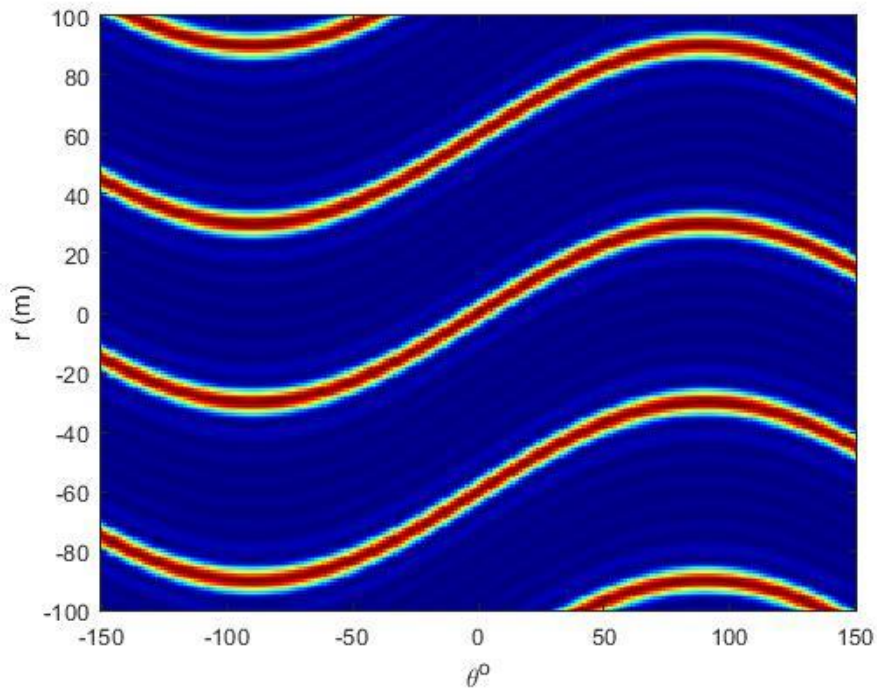

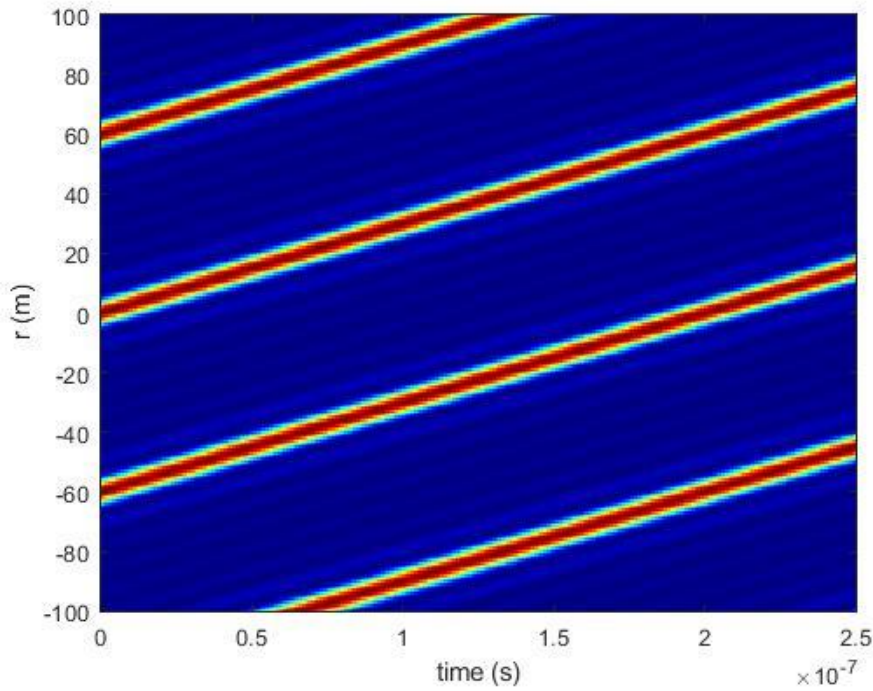*Figure 2.3.1 – Beampattern sFDA over range and azimuth, t = 0 s*

Figure 2.3.2- Beampattern of sFDA, over range and time

As it is possible to notice from the figure 2.3.1, figuring the beampattern over range and azimuth variables, an S-shape is provided. This represents a first example of simultaneous range and angle dependency of the array factor, providing an "intelligent" steering of the maxima. Several S-shapes are provided creating a periodicity in space that depends on the term Δf. In particular, the space distance between two S-shapes increases decreasing the value of Δf, viceversa increasing this value the S-shapes results closer one to each other. This behaviour is shown in the following figures:
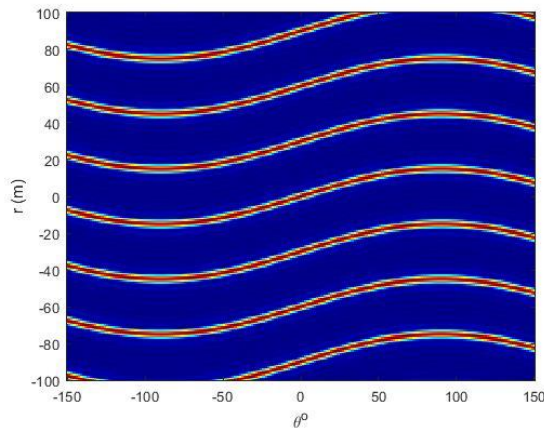

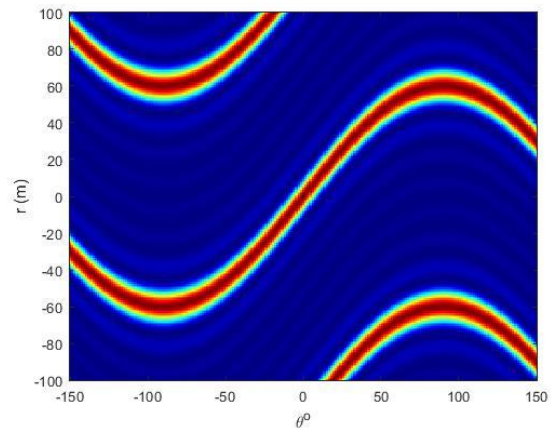*Figure 2.3.4 - Beampattern sFDA with $\Delta f = 10\ MHz$*

Figure 2.3.5 - Beampattern sFDA with $\Delta f = 2.5\ MHz$

In the figure 2.3.2 the temporal beahaviour of the sFDA is investigated for the first time, by considering a time window of 250 nsec. As it is possible to notice the beampattern results time-modulated, therefore when time passes the position of the maxima moves in space. This means that the different S-shapes move in space creating a sort of periodicity in time (the same point (r, q) of the space will be illuminated after a period T dependent on the value Δf): this represents an important drawback of FDA that needs to be taken under control in practical scenarios.

15

As conclusion of this study we can note that the sFDA represents a good solution in order to provide power in a specified position, but its behaviour is not interference - suppressing, i.e. it has not a single maximum in space. Also the time-modulated behaviour can be considered a defect, but here, due to the periodicity in time-space explained before, it can be considered under control.

Solution to these defects are provided in the next sections.

2.4.   FREQUENCY DIVERSE ARRAY WITH LOGARITHMIC DISTANCE DISTRIBUTION

In the frequency diverse array with logarithmic distance distribution, from here identified as logdistFDA, the only changed parameter with respect to the previous configuration, is the vector d_m collecting the distance of the m_{th} element from the element zero. In fact, the distance distribution follows a logarithmic rule in order to solve the first problem demonstrated by the sFDA, i.e. having maxima spanning a wide (r, q) area, thus providing a more restricted pointing area. Therefore, the set of parameters is:

$$f_m = f_0 + m * \Delta f; \ \ \Delta f_m = m * \Delta f \ \ for \ m = 0, \dots, M - 1$$

$$d_m = d_0 * \log (m + 1) \ \ for \ m = 0, \dots, M - 1$$

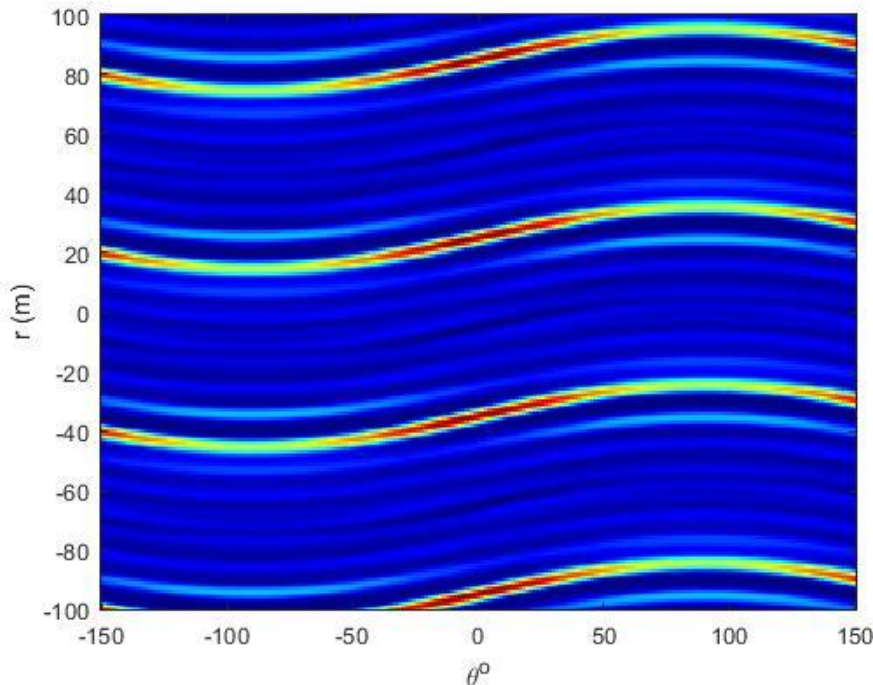The results are provided simulating in MATLAB a system with M= 8, $f_0 = 2.45 \ GHz, \Delta f = 5 \ MHz$:

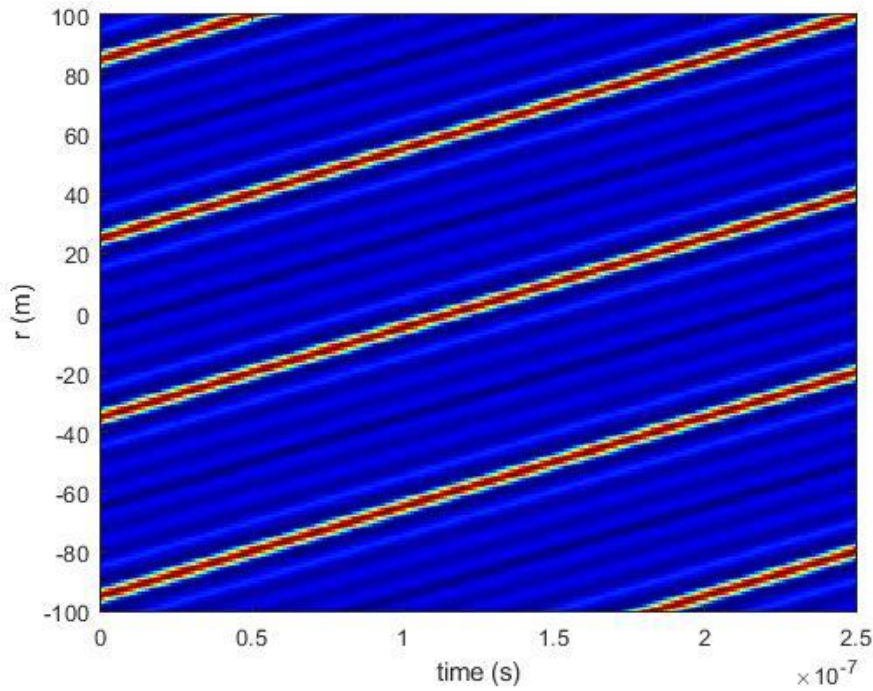*Figure 2.4.1 – Beampattern of logdistFDA over range and azimuth, t = 0 s*

Figure 2.4.2 – Beampattern of logdistFDA over range and time

As it is possible to see from the figure 2.4.1, with respect the previous configuration, the S-shape is eliminated in favour of an elliptical shape that provides a more-focused maxima in a specified angle range.

It is worth noticing that the periodicity in space is not eliminated since several maxima are found at different positions. The distance between two spots is again function of Δf, following the same rule as before.

It has to be noted, from the figure 2.4.2, that the time behaviour doesn't change with respect to the previous configuration, providing again a time-space periodicity that depends on the value of Δf.

An improvement has been reached, but from a practical point of view the logarithmic distance distribution imposes the realization of an *ad-hoc* array depending on the value of f_0 and the situation becomes more complicated due to the reduction of the d_m value mm

2.5. FREQUENCY DIVERSE ARRAY WITH LOGARITHMIC FREQUENCY DISTRIBUTION

Referring to the sFDA configuration, the frequency diverse array with logarithmic frequency offset configuration, from here identified as logfreqFDA, introduces a logarthmic distribution in the frequency vector, without changing the inter-element spacing. Therefore, the set of parameters can be given as in the following:

$$f_m = f_0 + \Delta f log(m+1); \ \ \Delta f_m = \ \Delta f log(m+1) \ \ for \ m = 0, \dots, M-1$$

$$d_m = m * d_0 \ \ for \ m = 0, \dots, M-1$$

17

The results in terms of beampattern 2D plot are provided again with MATLAB with M= 8, $f_0 = 2.45\ GHz, \Delta f = 10\ MHz$ in the following figures:
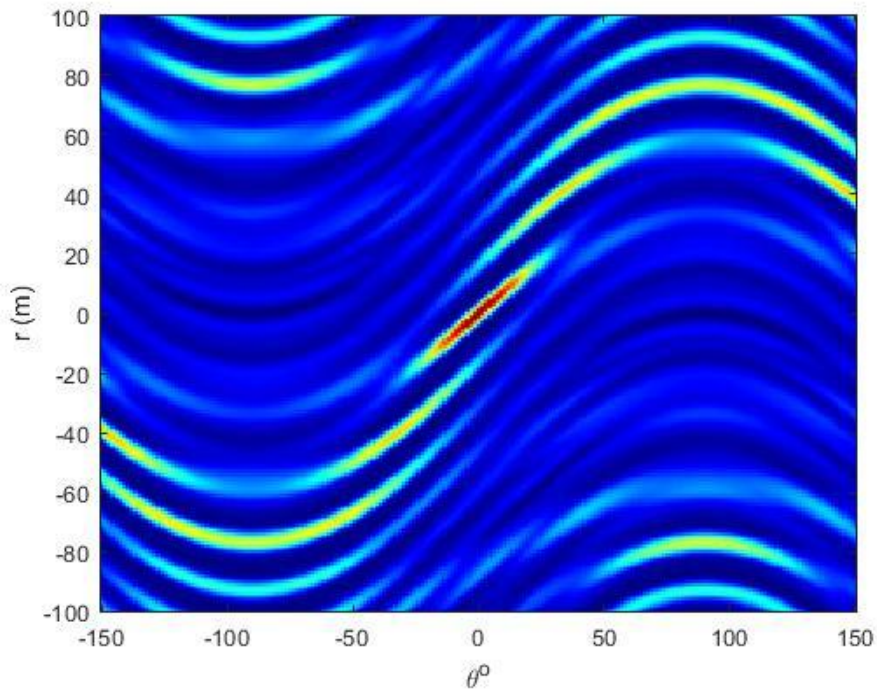

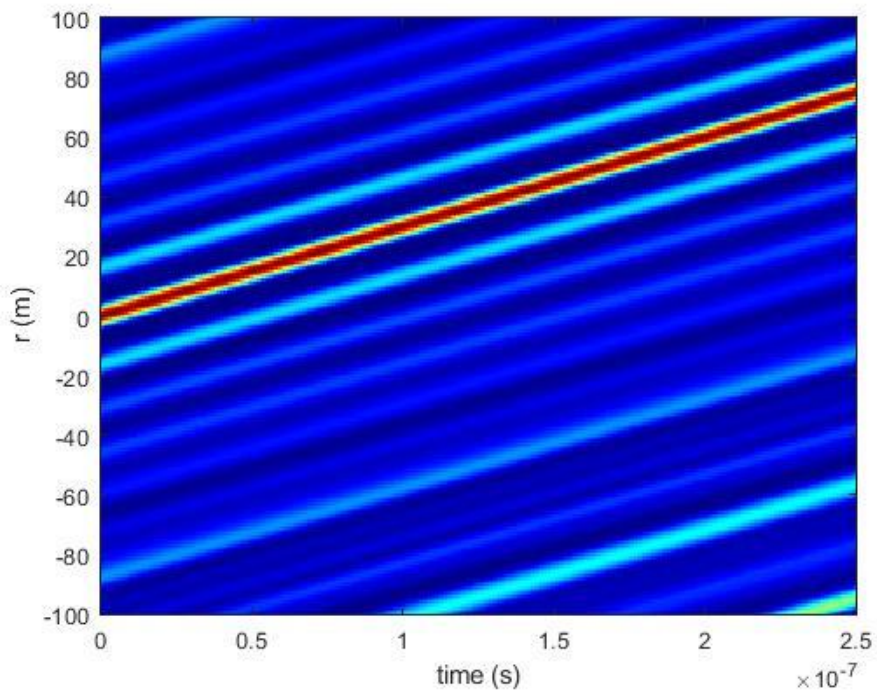*Figure 2.5.1 – Beampattern logfreqFDA over range and azimuth, t=0 s*

Figure 2.5.2 – Beampattern logfreqFDA over range and time

An improvement with respect to the previous configuration is reached. From figure 2.5.1 it is evident the presence of only one maximum with elliptical shape and the periodicity in space is suppressed.

From the figure 2.5.2 it can be evinced that the time-dependent behaviour has not been eliminated, since the movement of the maxima in space as a function of time is still present.

One can note that this configuration allows to steer the maxima in a desired location for t=0 changing the value of the complex weight a_m. In fact, selecting as target location the generic point (R_t, θ_t), the complex weight can be written as found in [8]:

$$a_m = \exp\left(\frac{j2\pi\Delta f R_t}{c} - \frac{f_0 d_m \sin(\theta_t)}{c}\right)$$

This represents a powerful tool in order to locate the maximum in whatever initial position. An example is provided in the following figure with $(R_t, \theta_t) = (30\text{m}, 30°)$:
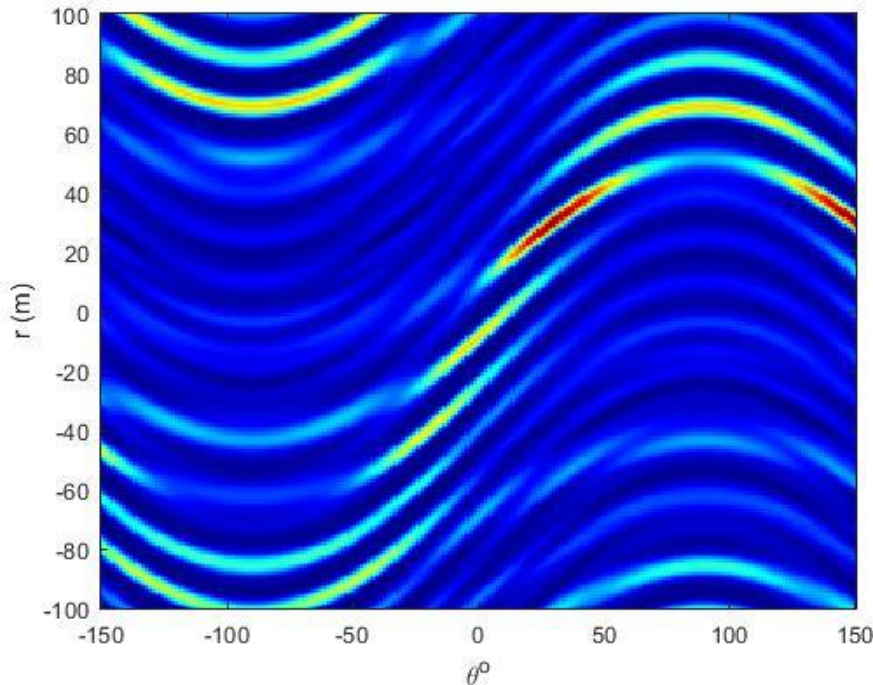

Figure 2.5.3 – Beampattern of logfreqFDA with $(R_t, \theta_t) = (30m, 30°)$, t = 0 s

From figure inspection, for t = 0 s the spot is located in the desired position. The behaviour in time is not eliminated and techniques to take this phenomenon under control have to be investigated further.

This configuration is object of this work and a possible design and implementation will be presented in detail in the next chapter.

Other configurations can be adopted for frequency diverse array in order to obtain the different properties, as the frequency diverse array with logarithmic frequency offset and logarithmic distance distribution. Other configurations can be obtained starting from the presented ones changing the set of signals in input to the radiating elements and technique can be adopted for eliminating the time-dependent behaviour in these cases, too. In this work they will not be studied since the focus will be on the logfreqFDA.

2.6. FIRST APPROACH IN PRACTICAL IMPLEMENTATION OF A logfreqFDA

It has been observed that for the realization of a system as logfreqFDA the use of M radiating elements that radiate at M different frequencies is needed. This implementation therefore requires:

- An array of M radiating elements in planar technology
- M different local oscillators to generate M different coherent sinusoidal tones
- M power amplifiers for every element
- A system to control the signal phases for beam steering purposes

For the purpose of this research, M = 8.

Designing this system in analogic electronic should be unfeasible due the following problems:

1) The logarithmic rule constraint for the generation of the sinusoidal tones is impossible to be rigorously applied: for example the vector of frequencies with M= 8, $f_0 = 2.45\ GHz, \Delta f = 10\ MHz$ results to be:

$$f_0 = 2450000000.00000 \text{ Hz}$$

$$f_1 = 2456931471.80560 \text{ Hz}$$

$$f_2 = 2460986122.88668 \text{ Hz}$$

$$f_3 = 2463862943.61120 \text{ Hz}$$

$$f_4 = 2466094379.12434 \text{ Hz}$$

$$f_5 = 2467917594.69228 \text{ Hz}$$

$$f_6 = 2469459101.49055 \text{ Hz}$$

$$f_7 = 2470794415.41680 \text{ Hz}$$

2) The use of 8 different local oscillators in order to generate the tones would increase a lot the cost of the entire system. Moreover, if free-running oscillators are adopted the control on the signal phase is lost, and, as a consequence, the array behaviour is lost, too, because of the uncoherent nature of the feeding signals. Very complex solutions, such as the use of injection-locked oscillators whose output signal phase could be controlled, are not convenient.
3) The introduction of the complex weights different from 1 would increase the complexity of the system, requiring to control also of the phase of the electromagnetic waves that excite the elements.

A solution to these problems is proposed:

In order to reduce the complexity given by the generation of tones with very precise frequencies (first problem), an approximation of them is required. In order not to lose the logarithmic relationship between the frequencies and to be able to replicate by simulation the corresponding situation, an approximation up to 10 kHz is introduced. The vector of frequencies thus results:

$$f_0 = 2450000000.00000 \text{ Hz}$$

$$f_1 = 2456900000.00000 \text{ Hz}$$

$$f_2 = 2461000000.00000 \text{ Hz}$$

$$f_3 = 2463900000.00000 \text{ Hz}$$

$$f_4 = 2466100000.00000 \text{ Hz}$$

$$f_5 = 2467900000.00000 \text{ Hz}$$

$$f_6 = 2469500000.00000 \text{ Hz}$$

$$f_7 = 2470800000.00000 \text{ Hz}$$

These frequency result less complicated to be generated, thus reducing a lot the complexity the system. The result of the approximated simulation is provided by MATLAB in the following figures, to be compared with Figs. 2.5.1 and 2.5.2: no significant differences are present.
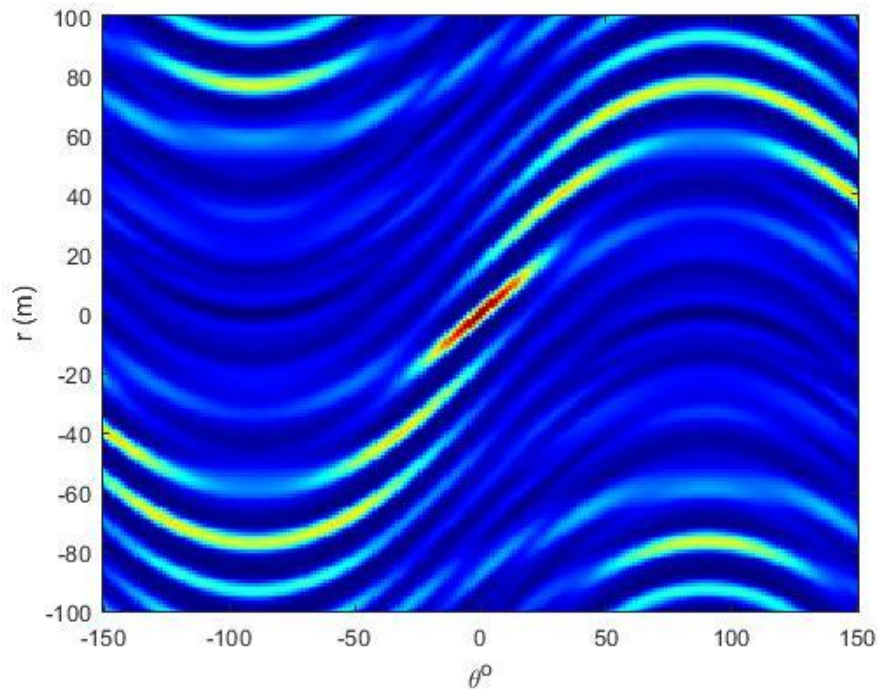

*Figure **Errore. Per applicare 0 al testo da visualizzare in questo punto, utilizzare la scheda Home.** - Beampattern approximated logfreqFDA over range and azimuth, t = 0 s*
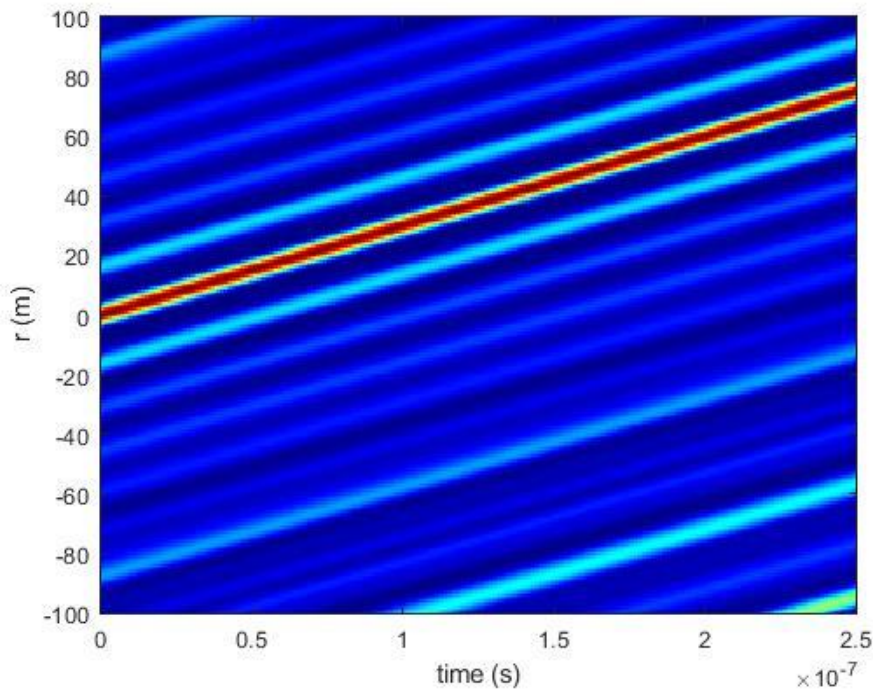
Figure 2.6.2 – Beampattern approximated logfreqFDA over range and time

To solve the second and third problem it is needed to move from analogic to digital domain, in particular with the use of the emerging technology called Software Defined Radio the generation and control of the signals is strongly reduced. This new technology allows to generate and control whatever signal in digital domain, and to modulate them to RF for feeding the elements in the correct way. The passage from analog to digital domain reduces a lot the complexity of the system, and allows to have two steps in the design procedure:

1) Nonlinear/electromagnetic co-design of the RF system, made of the array and its feeding network, explained in chapter 3

2) Design of the baseband system for the generation and control of the excitation signals, explained in chapter 4

The Software Defined Radio Technology, named also SDR, is a radio communication system where components that have been typically implemented via hardware (e.g mixers, filters, amplifiers, modulators, demodulators, detectors, etc.) are instead implemented by means of software on an embedded system. This technology allows to reconfigure the radio system via software, without he need to change the hardware. Even if this aspect will be treated in chapter 4, as a preview, an SDR platform running on a Xilinx board called ZCU111 RFSoC Ultrascale+ will be used in order to generate in baseband, digitally and dynamically, the desired signals to control the position of the maximum, therefore the beam-steering.

3. ARRAY CO-DESIGN, THROUGH ELECTROMAGNETIC AND NONLINEAR SIMULATION

In this chapter the section relative to construction of the frequency diverse array with logarithmic frequency distribution will be introduced. The first part will deal with the electromagnetic simulation provided by CST STUDIO SUITE, the second part will deal with the nonlinear simulation of the circuit containing the array through the in-house developed nonlinear simulator NONLIN used by the group of 'Campi Elettromagnetici' of DEI, University of Bologna.

As a model to simulate, and to be realized in the near future, it was chosen a frequency diverse array with logarithmic frequency offset with the following characteristics:

- 8 radiating planar monopoles
- Operating frequency $f_0 = 2.45\ GHz$
- Inter-element distance $d_0 = \frac{1}{2}\left(\frac{c}{f_0}\right) = 6.12\ cm$
- Incremental frequency offset $\Delta = 10\ MHz$
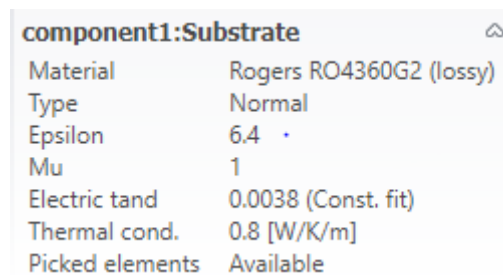- Planar technology with substrate Rogers RO4360G2 (Lossy)

3.1. ARRAY DESIGN AND ELECTROMAGNETIC SIMULATION

As mentioned before the first part introduces to the realization of the FDA array and is split in two parts:

1) Design and electromagnetic simulation of the single monopole in planar technology
2) Design and electromagnetic simulation of the FDA array

The characteristics are listed below:

- The monopole and the ground are realized in copper annealed with a thickness of 35 microns
- The substrate is Rogers RO4360G2 (Lossy) with thickness of 0.635 mm and the following electromagnetic characteristic:

Figure 3.1.1- Characteristics of the substrate

3.1.1. DESIGN OF THE SINGLE MONOPOLE FOR FDA

The design of the single monopole was performed using the electromagnetic simulator CST STUDIO SUITE. The final layout of the monopole resonating at 2.45 GHz results to be as in the following figures:
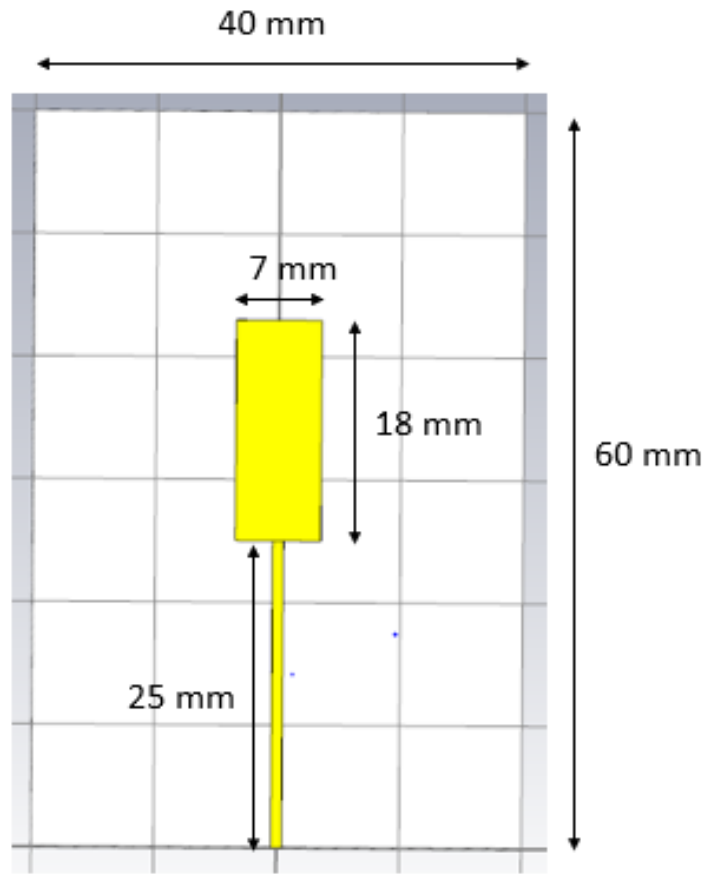
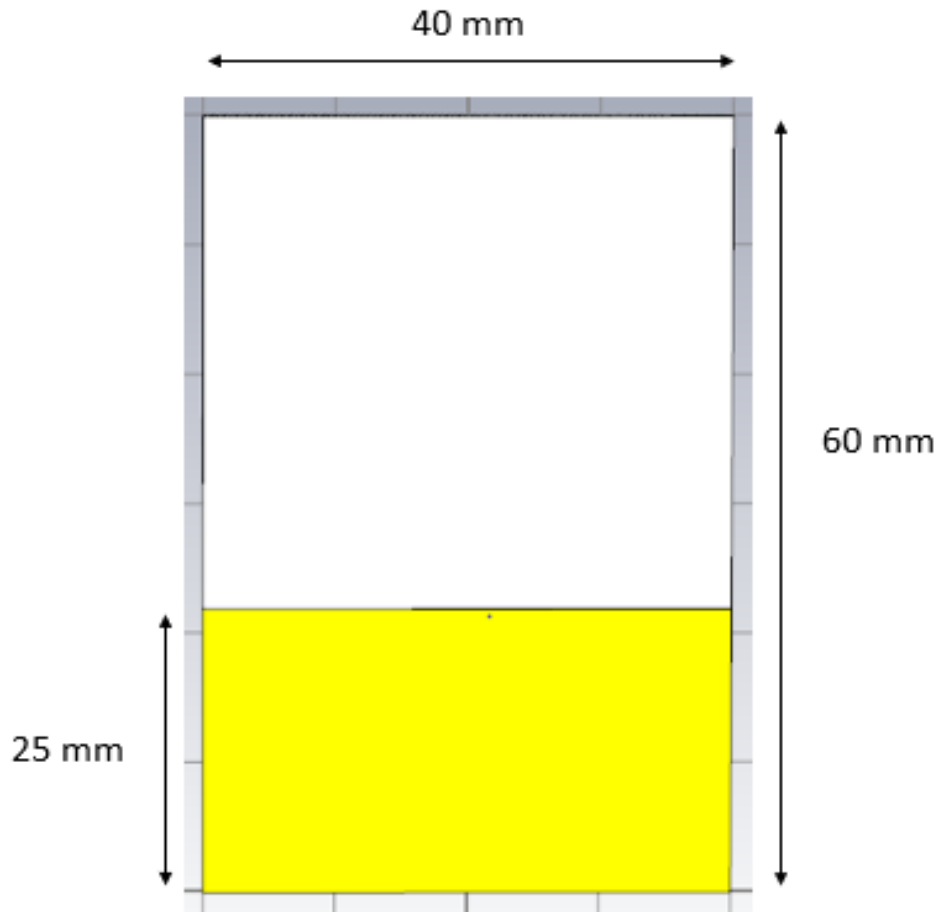*Figure 3.1.1.1 – Front view of FDA monopole*

Figure 3.1.1.2 – Back view of FDA monopole

The results of the transient electromagnetic analysis are provided using a waveguide port with width and height respectively 6 times the width of the microstrip and 5 times the height of substrate. They are reported in the following figures:
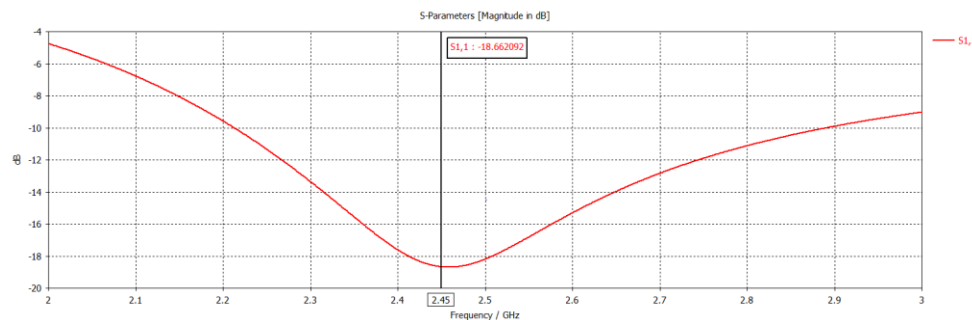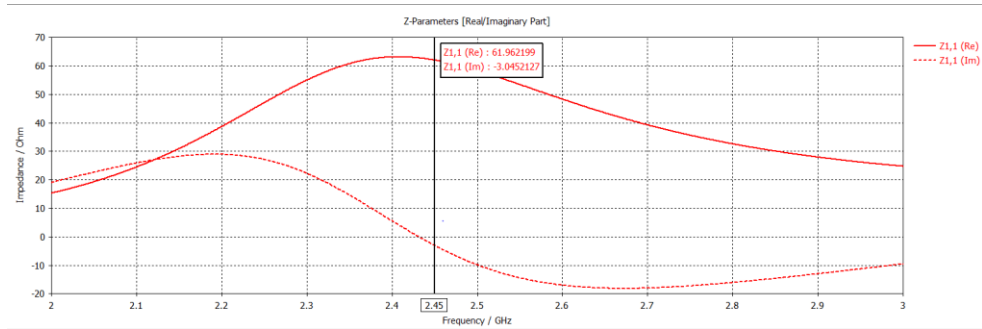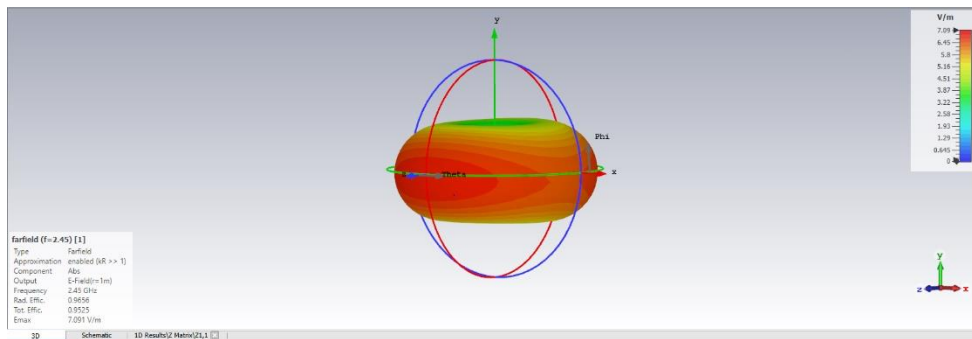

Figure 3.1.1.3 - |S11|

25

Figure 3.1.1.4 – Z11

Figure 3.1.1.5 – Farfield and E-field value

The results show good electromagnetic properties, in particular:

1) The value of |S11| at the operating frequency results to be about – 18 dB
2) The operating bandwidth, computed as the range of frequencies for which the value of |S11| is less than -10 dB result to be about 670 MHz (27%), confirming the narrowband nature of the monopole, but also the wide enough bandwidth for many standards working in this frequency band.
3) The values of the real and imaginary part of |Z11| suggest good input impedance properties (close to 50 ohm)
4) The radiation surface confirms the correctness of the simulation having the classical toroidal shape. Particular emphasis is given to value of radiation efficiency of about 95 %, confirming the very good properties of the substrate ROGERS RO4360G2

3.1.2. DESIGN OF THE ARRAY OF 8 ELEMENTS

The design of 8 element array has been carried out using CST in which the layout of the previous section was repeated 8 times, maintaining an inter-element spacing of l/2. The final layout of the array is reported in the following figure:
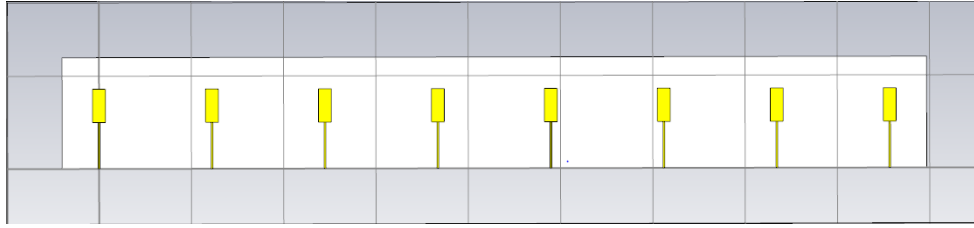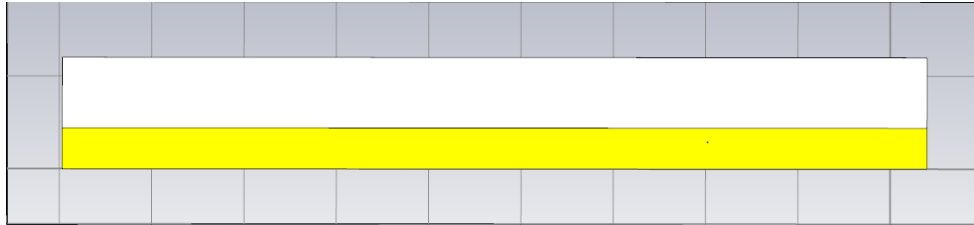
Figure 3.1.2.1 – Front view of the array

Figure 3.1.2.2 – Back view of the array

It has to be noted that using the transient analysis of CST STUDIO SUITE it is impossible to simulate an FDA system for which each element radiates at a frequency slightly different respect to the neighbours. Anyway, a transient analysis was performed in order to extract the field values of each element at the desired frequency to be used in the nonlinear simulator, as will be explained in the following section that will provide the results of an FDA array.

Therefore, the transient analysis by CST STUDIO SUITE provides the results of a standard phased array taking into account the electromagnetic coupling between the elements. Results of practical interest are provided in the following figures:
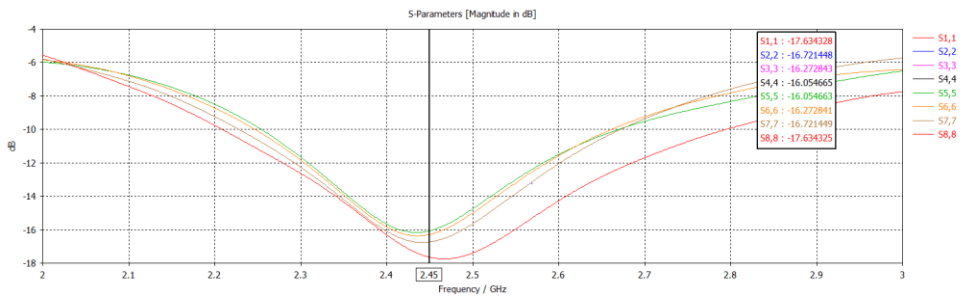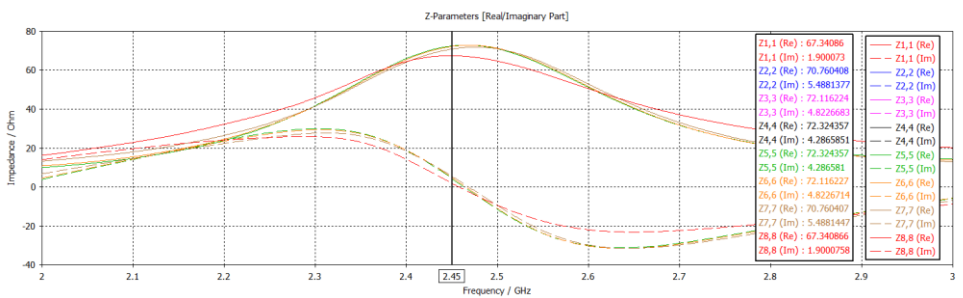

Figure 3.1.2.3 – |Sii|

Figure 3.1.2.4 – Zii

27

The values of the reflection coefficient at the different ports are good enough since |Sii| varies from -16 dB to -18 dB, offering a good matching condition for all the elements.

As a consequence, the values of Zii, both real and imaginary part, offer a good input impedance with a real part close to 50 ohm and greater than the imaginary part that results to be close to 0.

To conclude, the final array results to have good electromagnetic performance, even in this preliminary study, offering good quality of resonance and input impedance. The actual performance of the FDA architecture will be provided by the nonlinear simulator that will consider the electromagnetic description of the array through a touchstone file extracted from the CST simulation, and through the values of the farfield of all the elements, combining them with the real currents feeding the antennas.

3.2.   NONLINEAR SIMULATION OF FDA WITH LOGARITHMIC FREQUENCY OFFSET

This part will deal with the nonlinear simulation of the investigated FDA system, performing a Harmonic Balance analysis as done in [5] that involves all the set of frequencies used to excite the 8 elements. The system under investigation is represented in the following figure:
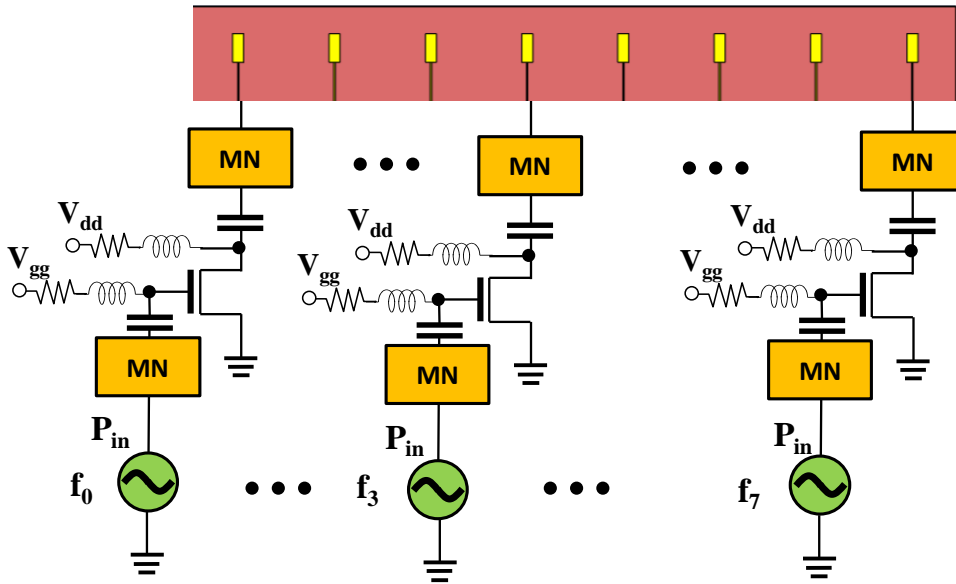

Figure 3.2.1 – Architecture for nonlinear simulation

The system under analysis is the logfreqFDA in which a non unitary value of the complex weights of the signals is considered. In fact that, for obtaining at t = 0 s a radiation pattern that shows its maximum in the point $(R_{target}; \theta_{target})$ the value of the coefficient a_m has to result:

$$a_m = \exp\left(\frac{j2\pi\Delta f R_t}{c} - \frac{f_0 d_m \sin(\theta_t)}{c}\right)$$

For what concern this analysis, values of $(R_{target}; \theta_{target}) = (30m, 0°)$ and $(R_{target}; \theta_{target}) = (30\ m, 20°)$ are considered, leading us to define the following complex weights:

m	$(R_{target}; \theta_{target}) = (30m, 0°)$	$(R_{target}; \theta_{target}) = (30m, 20°)$
0	0°	0°
1	-110.3°	-171.9°
2	35.8°	-87.3°
3	139.4°	-45.3°
4	-140.2	-26.5°
5	-74.5°	-22.3°
6	-19.0°	-28.4°
7	-29.1°	-41.8°

Each sinusoidal generator has (at its own frequency) an available power $P_{in} = -10\ dBm$ and phase obtained from the table above. As amplifiers, 8 single stage FET are introduced each of them providing a gain of 15 dB at each antenna port.

The numerical analysis of FDAs is a cumbersome problem, in fact a multi-tone, with M = 8, Harmonic Balance (HB) analysis cannot be carried out because of the rapidly increasing number of intermodulation products that have to be taken into account. Even commercial software are not able to perform this kind of analysis when the number of intermodulation products to be considered is ≥ 4. The only way to overcome this impairment is to perform a single-tone thus periodic analysis. Recalling that in the system under investigation the set of frequencies involved are:

$f_0 = 2450000000.00000$ Hz $\quad f_1 = 2456900000.00000$ Hz

$f_2 = 2461000000.00000$ Hz $\quad f_3 = 2463900000.00000$ Hz

$f_4 = 2466100000.00000$ Hz $\quad f_5 = 2467900000.00000$ Hz

$f_6 = 2469500000.00000$ Hz $\quad f_7 = 2470800000.00000$ Hz

In order to implement a single tone and periodic HB analysis a periodic regime has to be analyzed considering as fundamental tone the maximum common denominator of the frequencies involved. In the particular case of logfreqFDA this contribution results to be 100 kHz and a great number of harmonics are considered (100.000). This leads to have a frequency spectrum up to 10 GHz: this is needed because of the nonlinear nature of the radiating system, where superior harmonics (in this case up to the fourth harmonic) can play a significant role in the overall system behaviour. One can note that, by considering such an high number of spectral harmonics could results time and memory consuming, but the periodical nature of the regime (hence the mono-dimensional nature of the Fast Fourier Transform and Inverse Fast Fourier Transform used by HB) allows to handle hundreds of thousands of harmonics without high CPU time consumption.

Of course, from the far-field point of view, after the electromagnetic analysis of the array is performed, the extraction of the field pattern at the proper frequency for each antenna port must be carried out; after that, all the patterns are numerically combined after reaching the convergence of the HB analysis as a fast post-process procedure, because the actual value of the antenna feeding currents is needed.

Two investigations are provided:

- In the first one, the time instant has been fixed equal to 0 s, and the comparison between the beampatterns of desired spots and undesired spots is provided

- In the second one the time-dependent behaviour of logfreqFDA is investigated for the first at nonlinear level, providing a comparison between beampatterns at different time instants

The results of both the investigations are provided in the following figures:
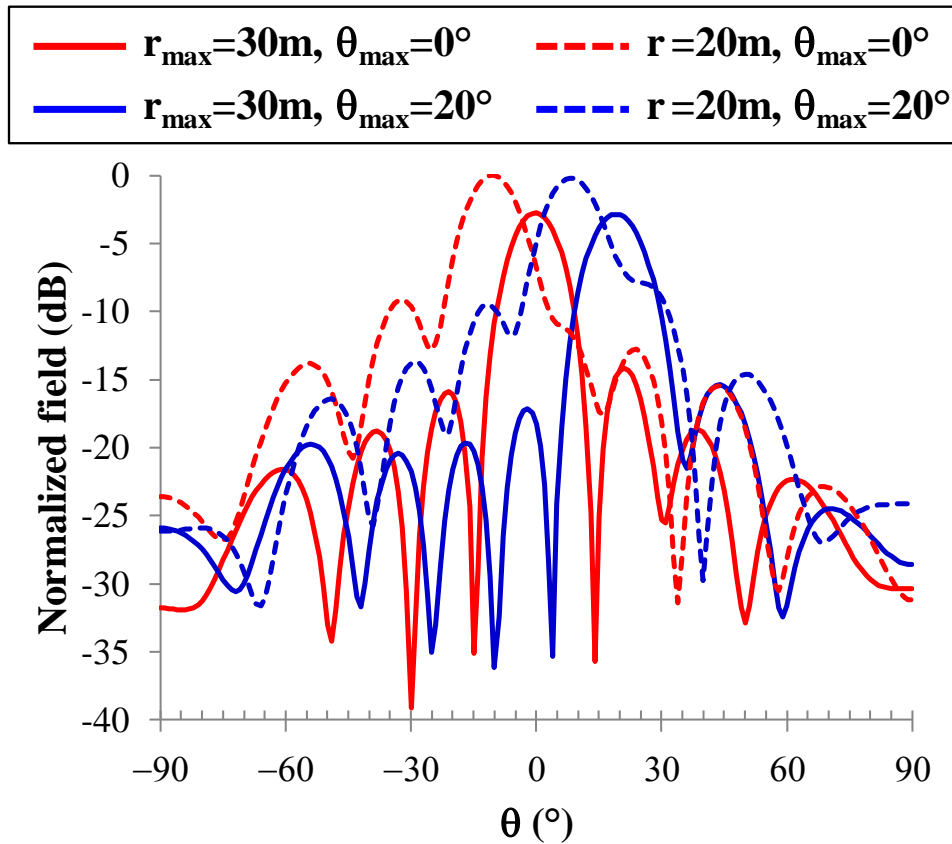

Figure 3.2.2 – Normalized radiation patterns for logfreqFDA with non uniform excitation, t = 0 s

As it can be noted, the figure 3.2.2 shows the normalized radiation patterns (in dB) for the two desired spots (solid lines) and the ones corresponding to the same phase excitation, but a lower distance (20 m) not corresponding to R_{target}. The effect of the proper phase distance is clearly visible: the maxima at 20 m are pointing in different q direction with respect to the desired ones, they are just few dBs higher than the desired ones (according to the Friis formula they should be stronger than they appear in the figure), and the side lobes at 20 m are less than 10 dB lower than the main lobe. Vice versa the patterns at the desired distance show a beautiful shape with a high side lobe level, thus confirming that the FDA is working properly just in those range and angle spots.

As mentioned before, the time-dependent behaviour of the logfreqFDA is investigated starting from the results provided with Matlab, considering, in this case, a uniform excitation ($a_m=1$). From the numerical simulation, showed in the following figure 3.2.3 we note that:

- the maximum of the array factor is around 10 m at t=35 ns
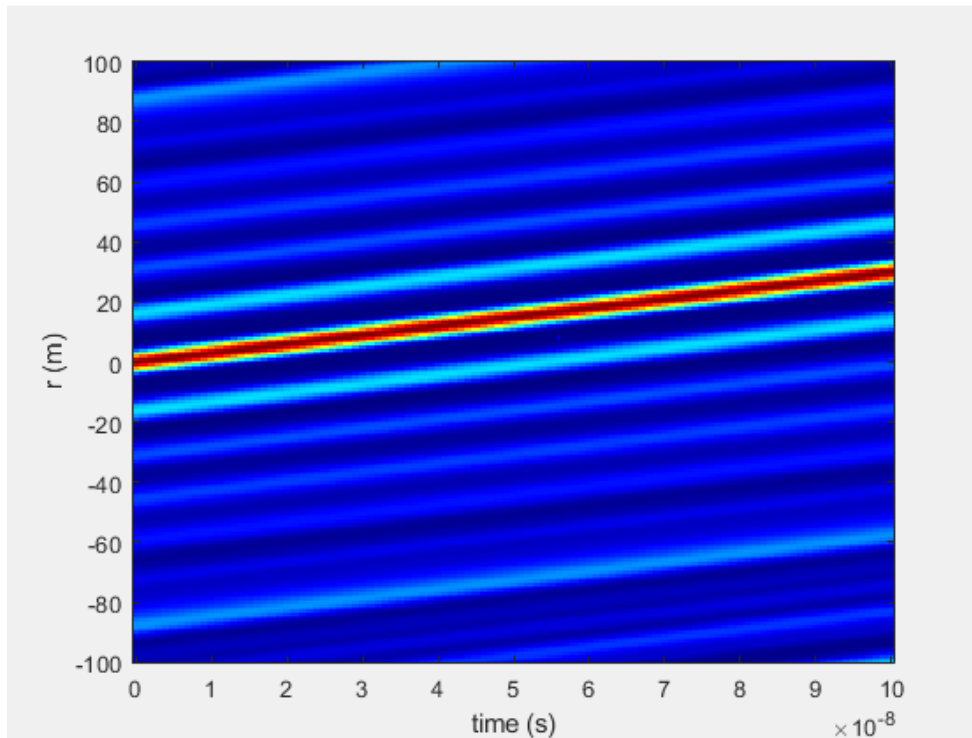- the maximum of the array factor is around 20 m at t=60 ns

Figure 3.2.3 – Numerical simulation of logfreqFDA with uniform excitation, time modulated behaviour

The results of the rigorous nonlinear/electromagnetic simulation in the aforementioned conditions are provided in the following figure:
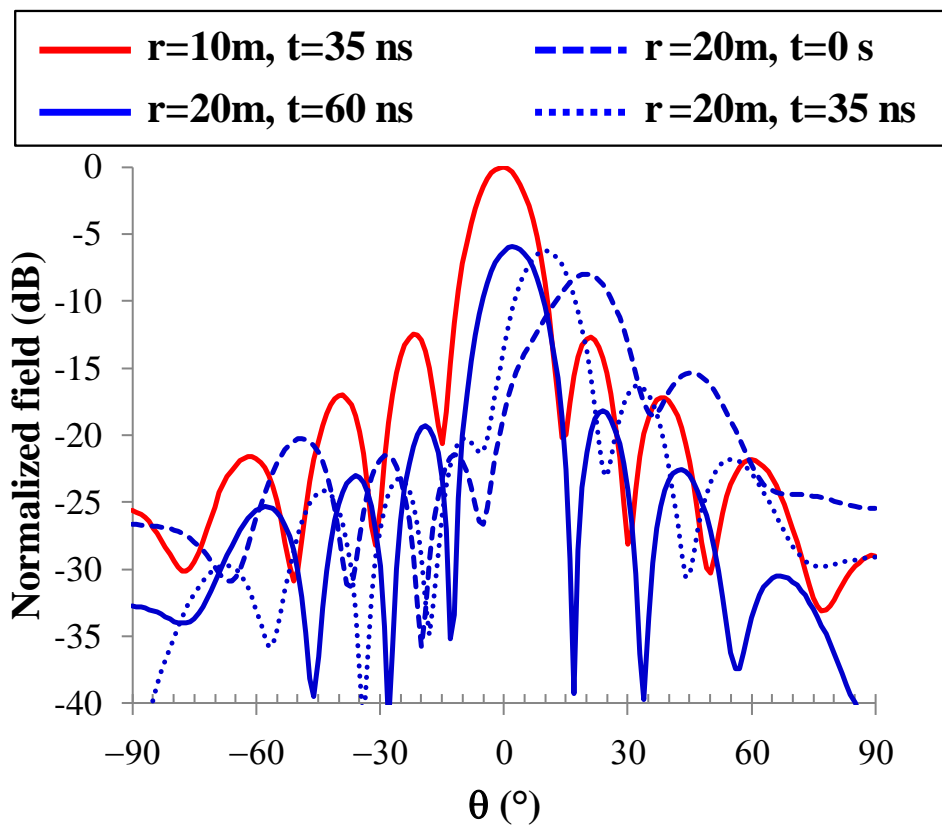

Figure 3.2.4 – HB simulation results

As it is possible to notice the solid lines correspond to the desired patterns at the proper (r, t) combination (i.e., (10 m, 35 ns) and (20 m, 60 ns)); the dashed lines are those of the undesired radiation patterns at the distance of 20 m, but at $t = 0$ and 35 ns, instants at which no maxima are present at 20 m (see Fig. 3.2.3). The shape and the strength of the desired patterns are sensibly better than the corresponding ones at the wrong time instant.

The analysis provided through harmonic balance technique confirm the results found with numerical linear evaluation showed in the previous chapter. An important consideration has to be done: the logfreqFDA system has the peculiarity of no-periodicity in time of its radiation mechanism. Countermeasures have to be taken to face this issue: a solution can be given by the possibility to create user-defined pulse as excitations at the array ports through modern SDRs. Practically speaking, the time periodicity can be imposed by switching off the system every Δt and applying a pulse just before the switch off. Using this technique, the term Δt becomes an added degree of freedom. The facts related to the creation of the set of signals using the SDR technology will be treated in the next chapter.

4. THE SDR SOLUTION FOR FDA SYSTEMS

As previously mentioned, this chapter will deal with the new emerging technology called Software Defined Radio (SDR) for which the components of the radio communication system, typically deployed in hardware, are instead implemented by means of software on an embedded system.

It is needed to recall that the configuration shown in the previous chapter with M local oscillators would result impossible to be realized given the high cost and the high difficulty in guaranteeing the coherent excitation of the M radiating elements. The SDR solution allows the user to completely define via software the entire system, in particular, for what concern this work, the signals generation and control.

The solution studied and offered in this work is represented by Zynq UltraScale+ RFSoC ZCU111 Evaluation Kit by Xilinx that supports 8 12-bit 4.096GSPS ADCs, 8 14-bit 6.554GSPS DACs, and 8 soft-decision forward error correction (SD-FECs), with Arm® Cortex®-A53 and Arm Cortex-R5 subsystems, UltraScale+ programmable logic, and the highest signal processing bandwidth in a Zynq UltraScale+ device. This kit provides a rapid, comprehensive RF Analog-to-Digital signal chain prototyping platform.

The features of the kit and the board are listed in the following figure:

Featured Xilinx Devices

Featuring the Zynq UltraScale+ XCZU28DR-2FFVG1517E RFSoC

12-bit, 4.096GSPS RF-ADC	8
14-bit, 6.554GSPS RF-DAC	8
System Logic Cells (K)	930
Memory (Mb)	60.5
DSP Slices	4,272
33G Transceivers	16*
Maximum I/O Pins	371

Figure 4.1 – Features of the Zynq Ultrascale+ RFSoC ZCU111

Before diving in the practical part and the characterization of the platform, a theoretical treatment about Digital Signal Processing is needed to deeply understand what follows next.

4.1. DIGITAL SIGNAL PROCESSING

With the introduction of the SDR technology, the design of the system under investigation moves from analog to digital domain. This assumption requires to be aware about criterions for correctly representing in digital domain an analog signal.

4.1.1. SAMPLING THEOREM

The most important theorem that allows us to represent an analog signal through samples is the Sampling Theorem by Shannon:

"If a function $x(t)$ contains no frequencies higher than B Hertz, it is completely determinated by giving its ordinates at series of points spaced by $1/2B$ seconds apart"

This important theorem suggests that the minimum sampling rate in order to create a unique relation between analog signal and its digital samples has to be at least 2 times the maximum frequency of the signal. The reason stands in the fact that when a passage from analog to digital domain is performed we can represent the digital representation in the frequency domain through the Fourier Transform. In particular, the Fourier Transform of a digital signal results to be the periodic repetition of the Fourier Transform of the analog signal with period f_s. Therefore, in order to avoid aliasing, i.e. a superposition in frequency of the repetitions, the sampling frequency f_s has to be at least $2f_{max}$. A graphical explanation is provided:
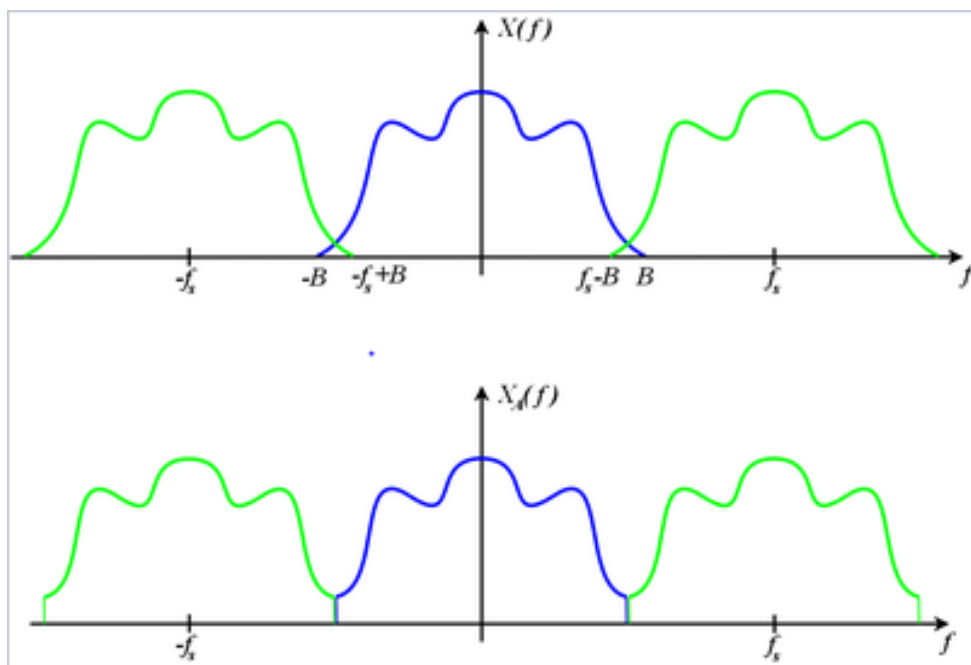

Figure 4.1.1.1 – Graphical representation of the sampling theorem, aliasing case
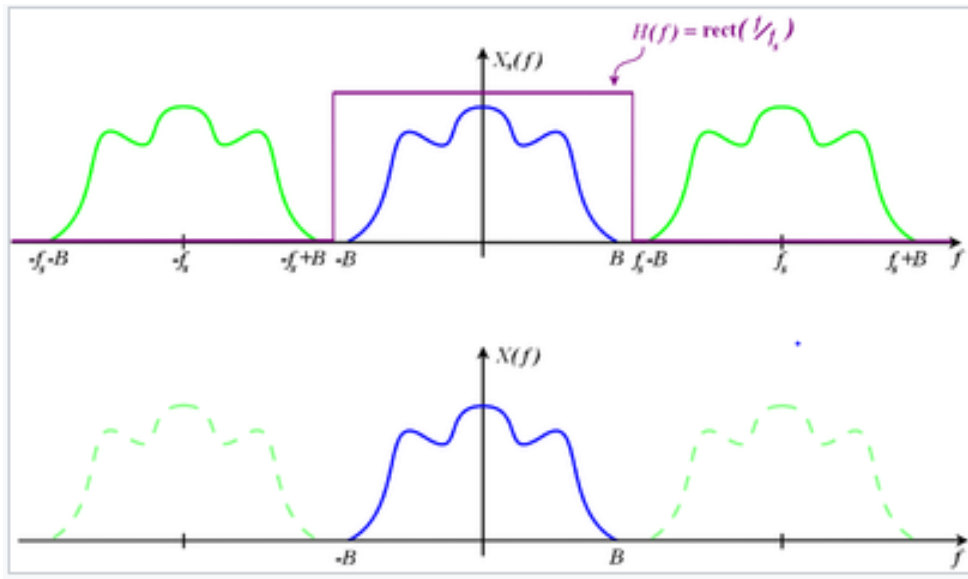
Figure 4.1.1.2 – Graphical representation of the sampling theorem, correct case

The spectrum of a digital signal can be divided in zones called *Nyquist Zones*, as shown in the following figure:
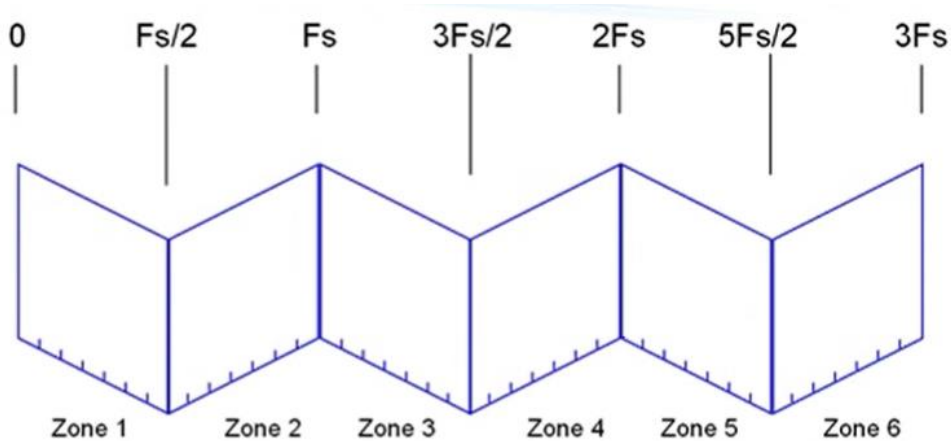

Figure 4.1.1.3 – Nyquist zones classification

4.1.2. REAL AND COMPLEX MODULATION

Another important classification, for what concerns the digital modulation scheme, is the real and complex modulation.

A real sinusoid is considered first:

$$x_{bb}(t) = \cos(2\pi f_{if} t)$$

We perform a mixing with another sine wave at higher frequency:

$$x_c(t) = \cos(2\pi f_c t)$$

35

After performing the calculation, the result is:

$$x(t) = x_{bb}(t)x_c(t) = \frac{1}{2}\cos(2\pi(f_c + f_{if})t) + \frac{1}{2}\cos(2\pi(fc - f_{if})t)$$

The first part represents the desired signal, instead the second one represents the undesired image signal.

This means that real signals have an equivalent mirrored positive and negative spectrum:
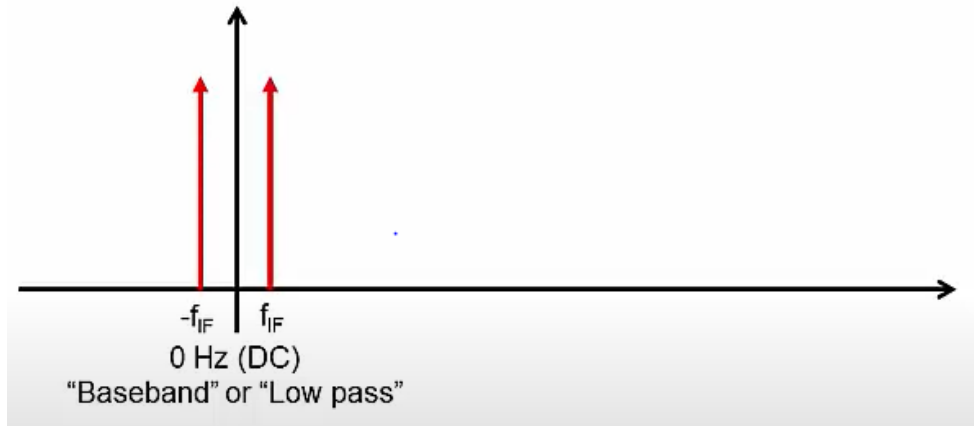

Figure 4.1.2.1 – Real sinusoid in baseband

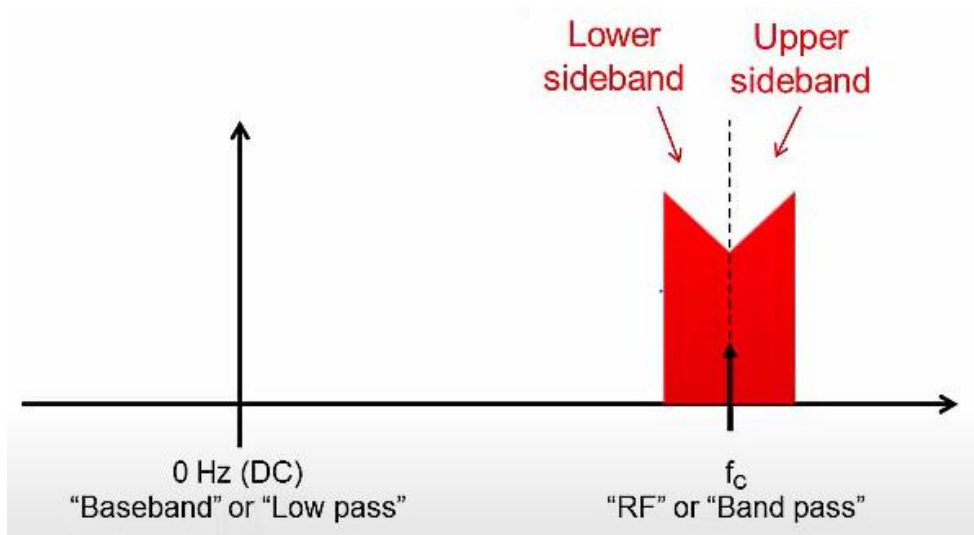When a real signal is mixed with another sine wave both components are mixed up:

Figure 4.1.2.2 – Real signal mixed up with carrier

This type of transmission is called "double sideband" (DSB) since the same information is transmitted in both sidebands.

Thing are different if a complex signal is considered:

$$x_{bb}(t) = \cos(2\pi f_{if}t) + j\sin(2\pi f_{if}t)$$

Considering the same carrier the result is:

$$x(t) = x_{bb}(t) * x_c(t) = \cos\big(2\pi(f_c + f_{if})t\big)$$

Only the desired components is present with a complex signal.

This is translated into the fact that complex signals have independent positive and negative spectra:
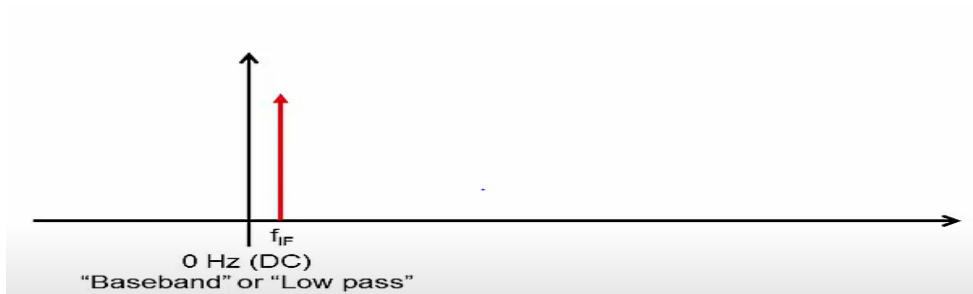

Figure 4.1.2.3 – Complex signal in baseband, positive spectrum

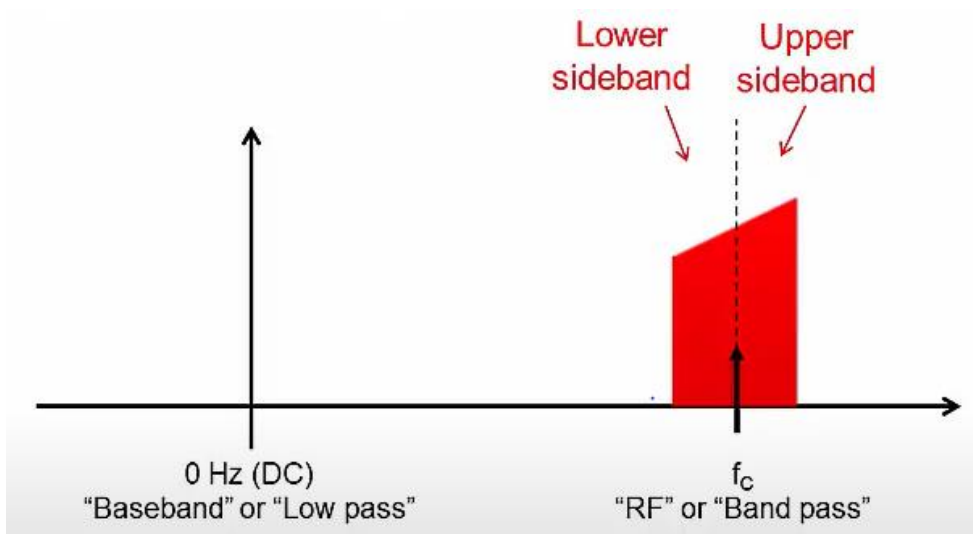*Figure 4.1.2.4 – Complex sinusoid in baseband, negative signal*

Figure 4.1.2.5 – Complex signal mixed up with carrier

37

This type of transmission is called "single sideband" (SSB) transmission since each sideband can transmit unique information.

It has to be clarified that in the real word the output signal will always have at RF a negative and positive component.

4.1.3. UPSAMPLING AND DOWNSAMPLING

These techniques are used to increase or reduce the sampling frequency in the digital circuit.
For what concern the upsampling, this procedure allows to increase the sampling frequency in order to adapt it to the sampling frequency required for the generation of the RF signal. Consider the following scheme:
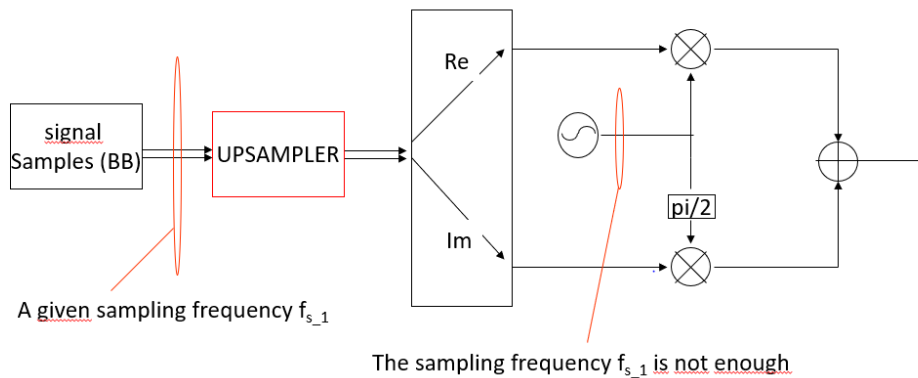

Figure 4.1.3.1 – From baseband to RF block scheme

The signal samples in baseband require a sampling frequency at least two times the maximum frequency of the relative baseband analog signal, that for sure will be lower than the maximum frequency the mixed signal at RF. Therefore, the sampling frequency needs to be increased and this is done through the upsampler: it increases the sampling frequency of a factor U such that:

$$f_{s_{new}} = U * f_{s_{old}} \quad with \ U = Upsampling \ factor$$

This is performed inserting U "zeros" between two samples every $f_{s_{new}}$. This introduces a power loss of U that needs to be counterbalanced with a power amplifier that increases the signal level about the same quantity. It has to be noted that FIR filters are needed after the upsampler in order to eliminate the images.

This procedure is needed in particular to adapt the data rate of the embedded system to the sampling rate of DAC in order to obtain the correct output analog signal.

The downsample is the inverse procedure for which we decrease the sampling frequency in order to adapt it to the operating frequency of the embedded system. This is performed considering only samples with sampling frequency:

$$f_{s_{new}} = \frac{f_{s_{old}}}{D} \quad with \ D = downsampling \ factor$$

From the implementation point of view, a FIR filter before each step of downsampling is needed to eliminate possible interferences.

This procedure is needed, in particular, to adapt the rate of the incoming signal from ADC to the operating frequency of the embedded system.

4.2.   ZYNQ ULTRASCALE+ ZCU111 EVALUATION KIT

As previously mentioned, the SDR platform is represented for this implementation by the Zynq UltraScale+ ZCU111 Evaluation kit by Xilinx that offers a rapid, comprehensive RF Analog-to-Digital signal chain prototyping platform.

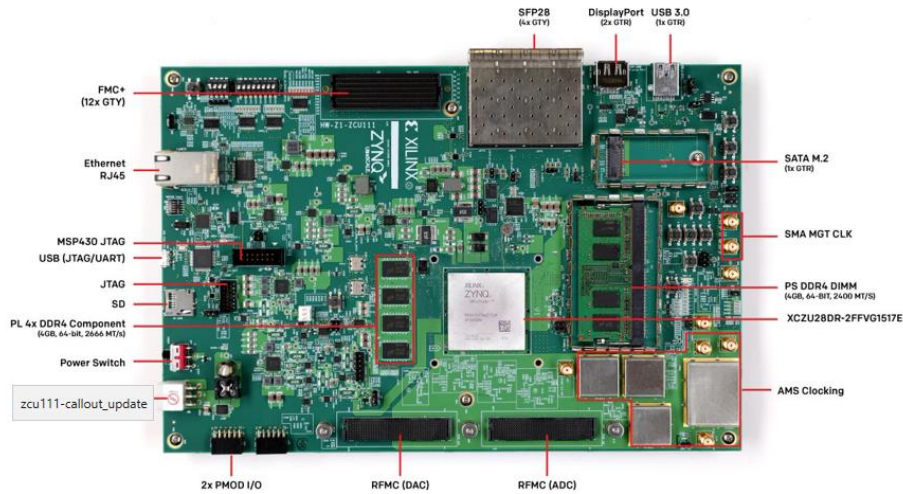The front view of the board is reported in the following figure:

Figure 4.2.1 – Zynq Ultrascle+ RFSoC ZCU111 board

It can be noticed that the functionality of the board can be divided in 3 subsystems:

- The Processing System (PS) that comprehends Arm® Cortex®-A53 and Arm Cortex-R5
- The programmable logic (PL)
- The Data Converter

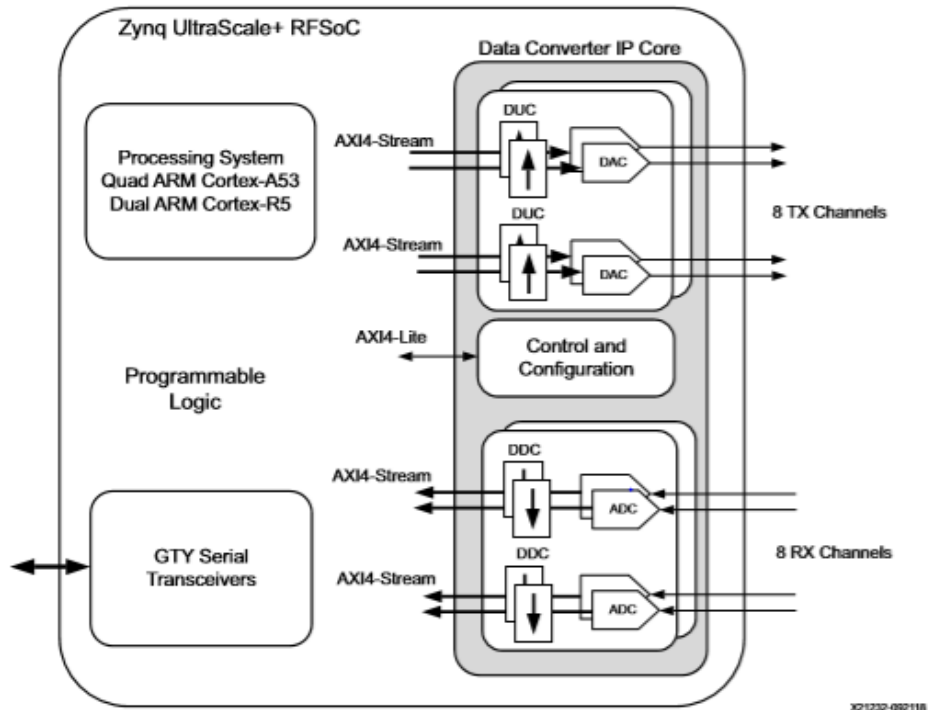The system overview is reported in the following figure:

Figure 4.2.2 – Overiew of Zynq Ultrascale+ RFSoC ZCU111

The focus of the present thesis work is on the last subsystem, i.e. the Zynq Ultrascale+ RFSoC RF Data Converter. This subsystem allows to generate and control the baseband signals and directly convert them at RF and vice versa, using the 8 6.554 GSPS RF-DACs and the 8 4.096 GSPS ADCs. Therefore, up to a maximum of 8 channels can be simultaneously controlled by this board: this explains also why an 8-monopole FDA has been designed in the previous chapter.

Several tools are provided in order to control this subsystem: in this research activity the Zynq Ultrascale+ RFSoC RF Data Converter Evaluation Tool offered by Xilinx has been used.

It is worth noticing the fact that, in order to extract the signal from the DACs or passing them to the ADCs, a couple of RFMC connectors are provided. These connectors, produced by Samtec, are called LPA (Low Profile Array) pins and provides a connection using a matrix of pins as shown in the following figure:

*Figure **Errore. Per applicare 0 al testo da visualizzare in questo punto, utilizzare la scheda Home.***RFMC connectors (LPAx connectors)*

Therefore, the only way to interact with the ZCU111 is through an external board that have this type of connection. This will be treated later in this section.

4.2.1. RFSoC RF DATA CONVERTER EVALUATION TOOL

This part will deal with the tool used for controlling the entire chain digital to analog and analog to digital of the data converter subsystem of the ZCU111. It is a graphical tool that allows the user to generate the signals and set the blocks in order to perform the up and down conversion.
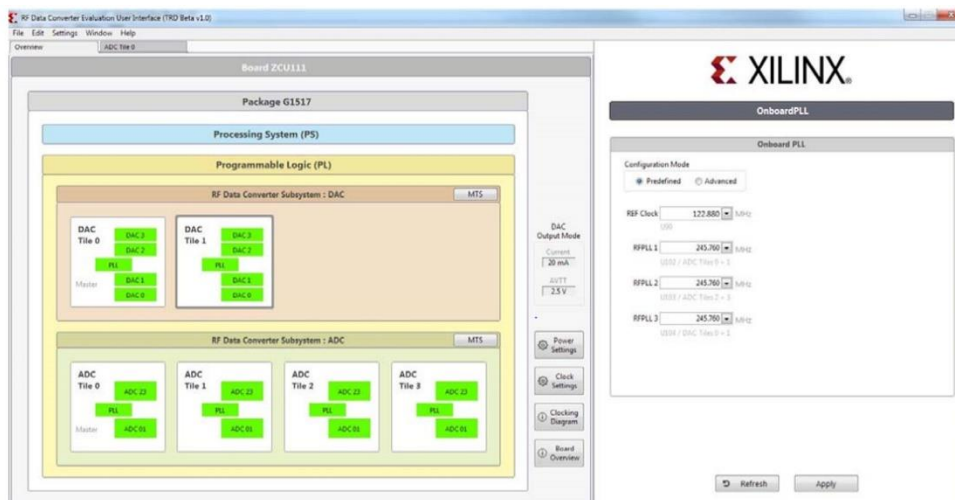

Figure 4.2.1.1 – RFDC evaluation tool

The figure shows the main window of the tools in which the DAC and ADC subsystem are highlighted. The main window allows to set several parameters as the DAC output mode, clock settings and power settings. A detailed explanation will be provided later in this section.

As it is possible to notice, the DAC subsystem is divided in 2 tiles, each one containing 4 DACs and one PLL able to set the sampling frequency. The ADC subsystem is divided in 4 tiles, each one containing 2 ADCs and one PLL.

RF-DAC

Each RF-DAC tile includes a complete clocking support structure with a PLL and the necessary synchronization logic. Every RF-DAC in a tile has a highly configurable FIFO allowing the internal interconnected logic to have direct high-speed access to the RF-DAC (see figure below).
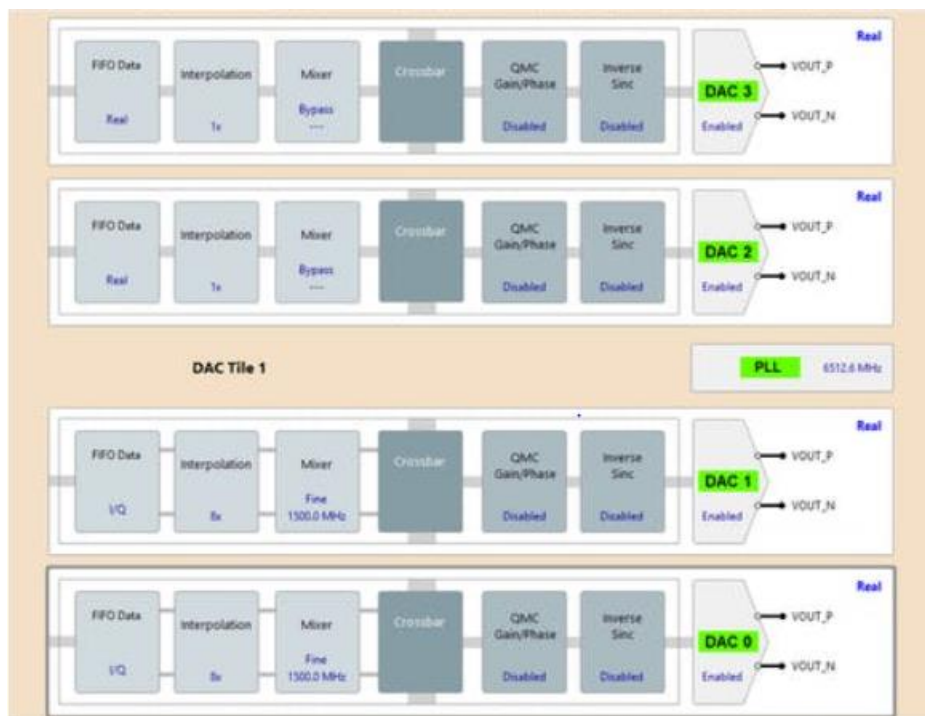

Figure 4.2.1.2 – RFDC evaluation tool, DAC subsystem

Each RF-DAC in a tile has a number of optimized DSP features that can be used to implement Digital Up Conversion (DUC) and transmit signal filtering. These features are:

- Signal interpolation function - interpolations x1 (bypass), ×2, ×4, or ×8 are supported

- Coarse mixing (quarter and half rate) or fine mixing with a 48-bit frequency resolution

- numerically controlled oscillator (NCO)

- Compensation functionality containing a quadrature modulator correction (QMC) block with coarse delay adjustment block

- Signal conditioning containing an inverse sinc FIR filter

The explanation of the blocks is given in the following:

42

FIFO DATA: The data interface between the RF-DAC tiles and the PL, that is implemented using parallel data streams, using the AXI4-Stream protocol. These data streams are input to gearbox FIFOs that provides a flexible interface between the user application and the RF-DAC tile. The maximum interface width is 256 bits per stream, representing up to 16 16-bit words.

INTERPOLATION: Interpolation filters are required to implement the up-sampling and filtering portions of the DUC process. The implemented filter operation consists of three low pass FIR filters, each with a predetermined, fixed set of coefficients, shown in the following figure. Each filter block can be bypassed and the output of each filter block can be routed to the output of the filter. This allows the creation of the following signals:

- 1x—all filter stages are bypassed

- 2x—interpolation using a single stage

- 4x—interpolation using two stages

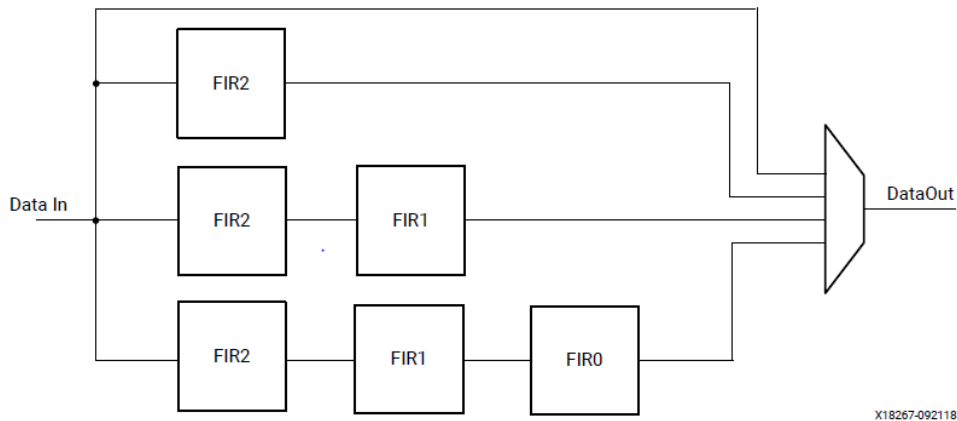- 8x—interpolation using all three available stages

Figure 4.2.1.3 – Interpolation block

MIXER: The mixer function has three modes, bypass (no mixing), coarse mixing or fine mixing. Fine mixing automatically enables the NCO which is used to generate the carrier frequency. The mixer supports full quadrature mixing, with both real to I/Q and I/Q to I/Q modes supported.
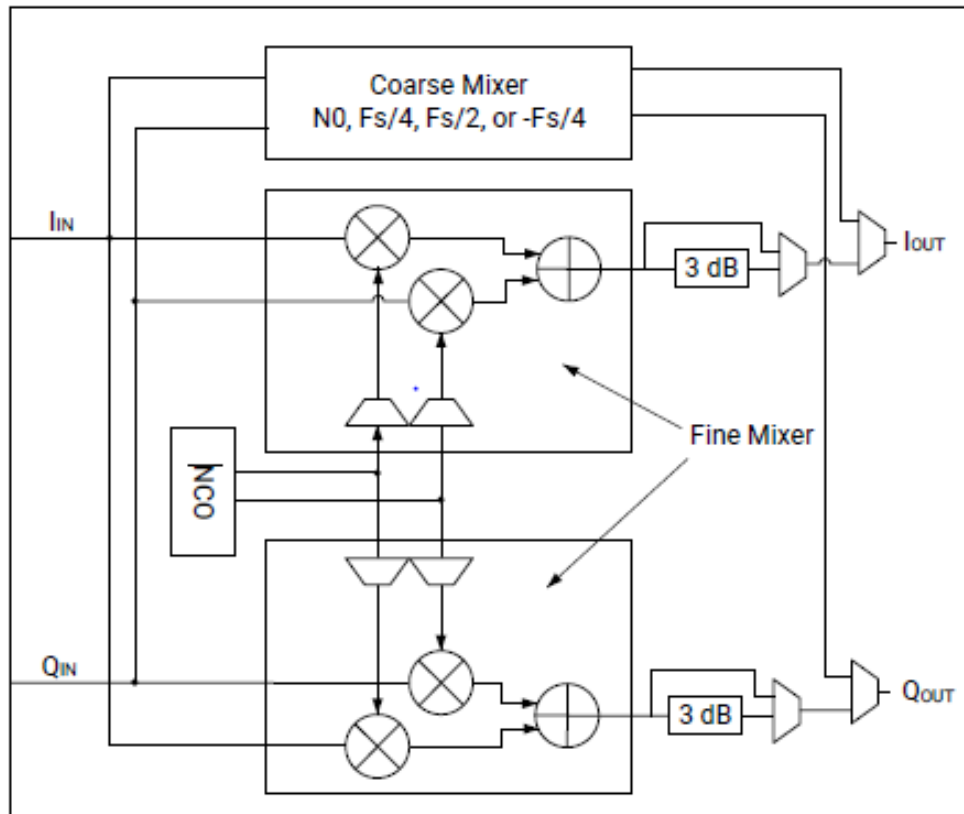
Figure 4.2.1.4 – Mixer block

Coarse Mixer:

- The coarse mixer allows the data to be mixed with a carrier of 0, Fs/2, Fs/4, or –Fs/4.
- Mixing with a 0 carrier bypasses the mixer component.

Fine Mixer:

- The fine mixer allows the data to be shifted up or down in frequency by an arbitrary amount.
- The frequency shift amount is obtained by programming the mixer frequency generated in the NCO. The fine mixer also supports 18-bit phase adjustment.
- To manage potential overflow, the fine mixer output includes 3 dBV attenuation, as shown in the figure above

CROSSBAR: It allows to select the operating mode (explained later in this section)

QMC GAIN/PHASE: When using an external analog quadrature mixer device, a pair of converters (either RF-ADC or RF-DAC) must be used to handle the I and Q data-paths after conversion. Due to external events or circumstances, errors or imbalances can be introduced in the analog I and Q signal paths which, if not corrected, can lead to system performance degradation. The necessary corrections to restore any system from degrading are accomplished using the quadrature modulator correction (QMC) circuit.

DAC and INVERSE SINC: Each RF-DAC in a tile has its own differential analog current output buffer/driver. The output currents are complementary; the sum of the two currents always equals the full-scale current of the RF-DAC. The RF-DAC output current is configurable, with an option of operating in either 20 mA or 32 mA modes. In the 20 mA mode, set the DAC_AVTT to 2.5V and in the 32 mA mode, set it to 3.0V to maintain the linearity performance. Each RF-DAC can optimize its response in the first or the second Nyquist zone by using the normal mode or mix mode feature. The trasfer function of the DAC is provided:
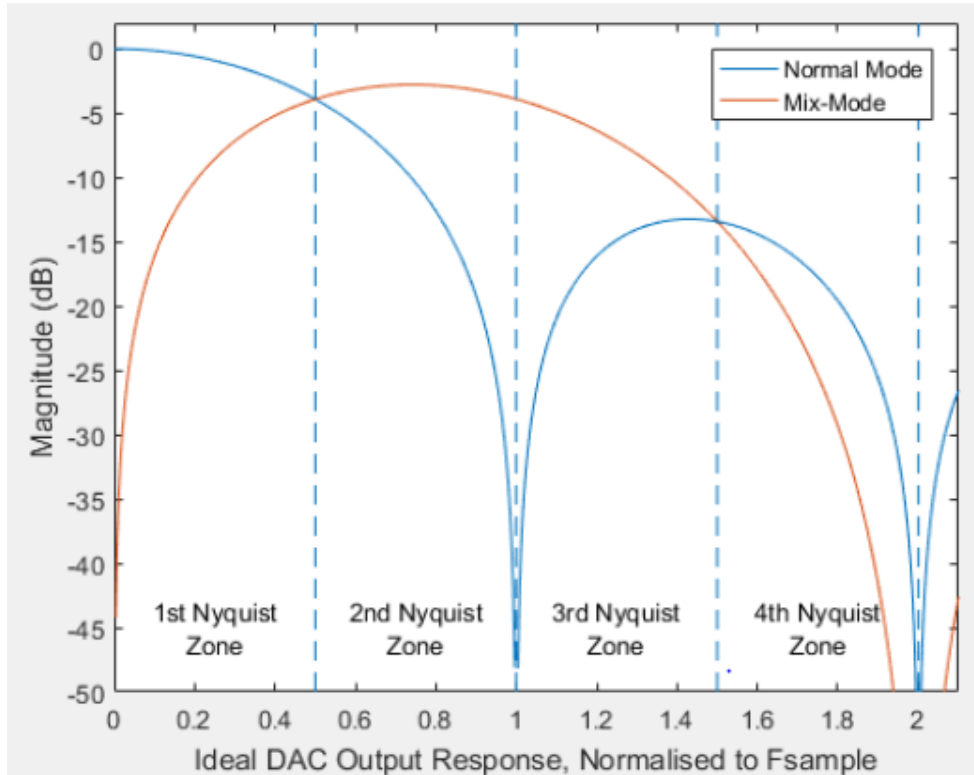

Figure 4.2.1.5 – DAC transfer function

For normal (non-mix mode) operation, the blue line represents the ideal RF-DAC output roll-off sinc response. As can be seen, an output image in the second Nyquist zone in this mode would be severely attenuated. An inverse sinc filter is available to compensate for the roll-off in the first Nyquist zone for this mode.
In RF-DAC mix-mode, the red line represents the ideal RF-DAC output response. In this mode, the output power of the image in the second Nyquist zone is significantly increased, and it also has an approximately flat response across the majority of the zone.

The analog output response of the RF-DAC follows a characteristic sinx/x, or sinc shape. For applications that require flat-output response over a wide bandwidth, an inverse sinc filter is available to achieve this. The inverse sinc filter is an 11-tap FIR, which provides a flat-response with less than ±0.05 dB of ripple up to 89% of Nyquist, or ± 0.033 dB of ripple up to 80% of Nyquist. The following figure shows the inverse sinc performance.
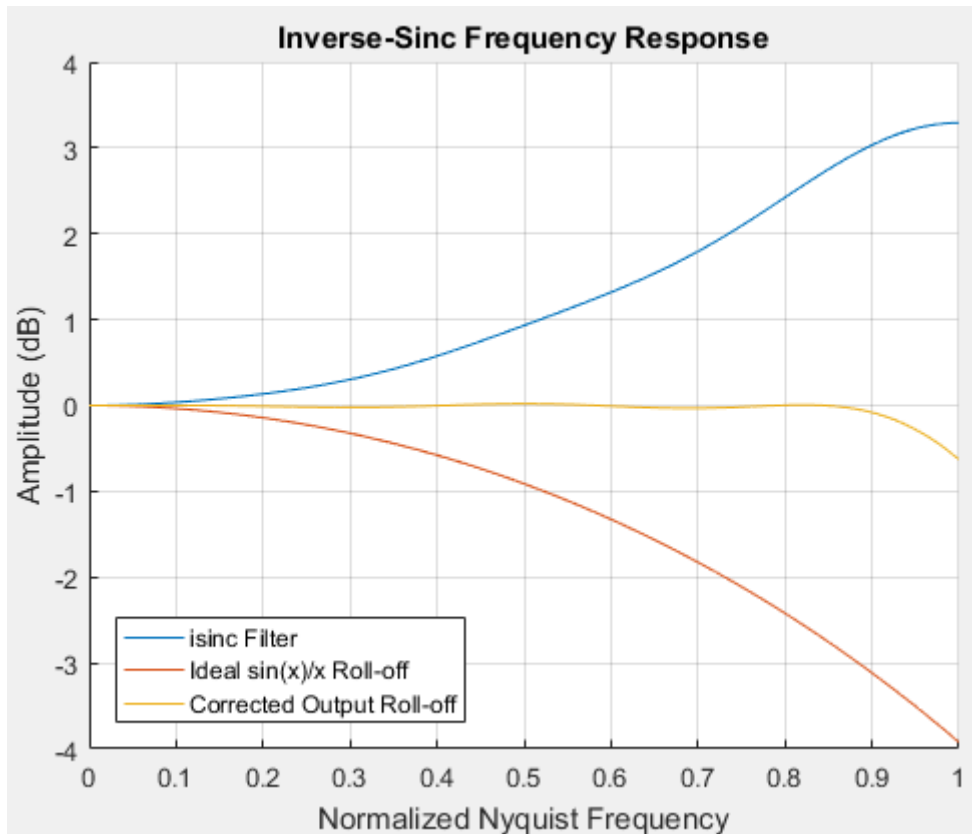
Figure 4.2.1.6 – Inverse Sinc transfer function

The line in blue represents the frequency response of the filter itself. As can be seen, it increases with frequency to compensate for the sinc response of the output, as shown by the red line. The composite output response is given by the yellow trace, and shows a flat pass-band up to 89% of Nyquist.

Finally the RF-DAC can be configured in several modes:

- Real Input to Real Output

Figure 4.2.1.7 – Real input to real output configuration

- I/Q Input to Real Output

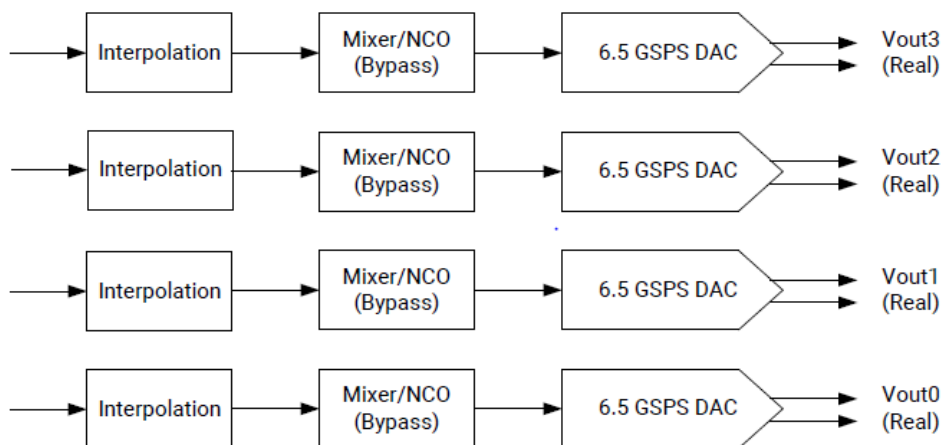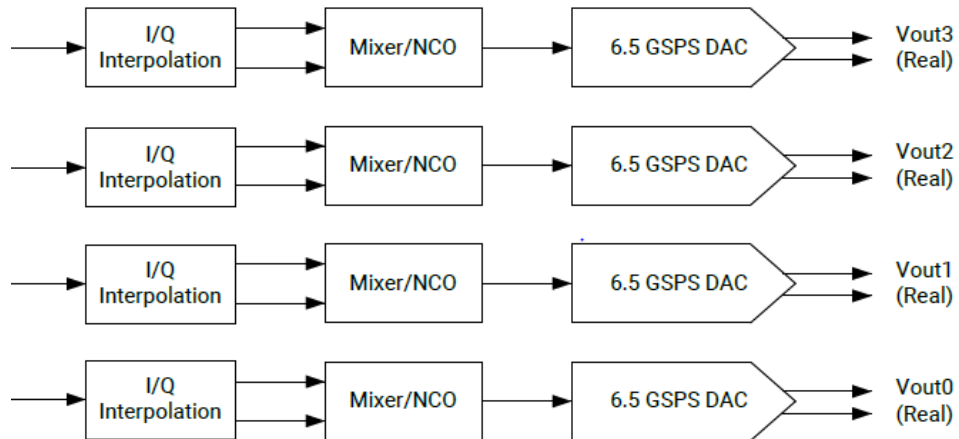*Figure 4.2.1.8 – I/Q input to real output configuration*
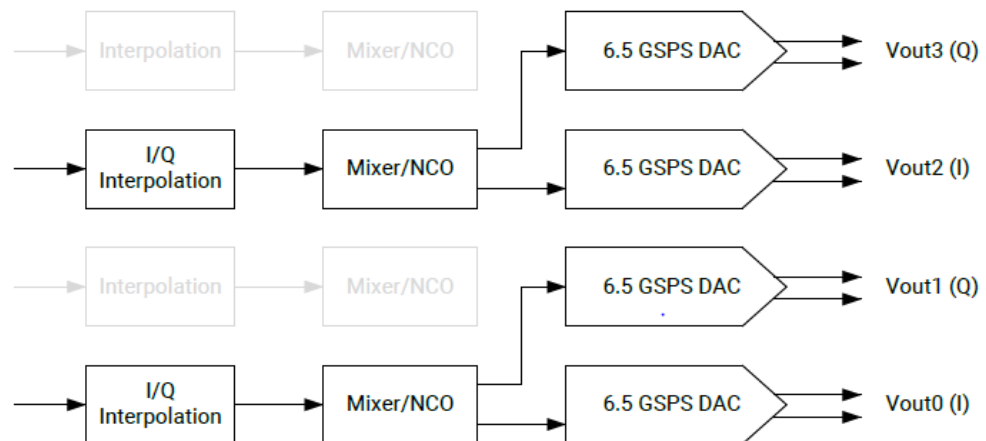
- I/Q Input to I/Q output

Figure 4.2.1.9 – I/Q input to I/Q output configuration

RF – ADC

Every RF-ADC in a tile has its own dedicated high-performance input buffer and includes features optimized for direct conversion applications including quadrature modulator correction (QMC), full complex mixers, and decimation filters.

Figure 4.2.1.10 – ADC subsystem

An RF-ADC component in a tile has integrated DSP features which can be enabled by the user to pre-process the sampled data from the RF-ADC device before it is passed to the PL. The different DSP function blocks are as follows:

- Detection functionality—containing a dual level programmable threshold that provides two flags to the internal interconnect logic, and is asserted when the absolute value of the RF-ADC is greater or smaller than the programmed threshold values.

- Compensation functionality—containing a quadrature modulator correction (QMC) block with a coarse delay adjustment block

- Digital down converter (DDC)—consists of mixing followed by decimation

- Mixer—coarse (quarter and half rate) and fine (NCO with 48-bit frequency resolution)

- Signal decimation functionality—decimation by 1 (bypass), 2, 4, or 8 is supported

The functionalities of the blocks are explained in the previous section (RF – DAC)

4.2.2. LOOPBACK TEST

As first experimental characterization for checking the correct working of the board a loopback test is performed. This experiment consists in generating sinusoidal tones and receiving them with the use of an external board that will be introduced later in this section. The visualization is provided through the DAC and ADC windows in the RF Data Converter Evaluation Tool (only baseband visualization is provided).

Before starting, a preliminary analysis about the signals that can be handled in this test has to be done. The performance is strictly related to the ADC characteristic, remembering that the maximum sampling rate reached for these components are 4.096 GSPS, a maximum RF signal can be correctly sampled. Following the Sampling Theorem, the maximum value of the frequency of the signal has to be:

$$f_{MAX} = \frac{F_s}{2} = 2.048 \; GHz$$

The equipment needed for these experiments is provided:

- ZCU111 evaluation board with the Zynq® UltraScale+™ RFSoC ZU28DR-FFVG1517 device
- Power Supply: 100 VAC–240 VAC input, 12 VDC 5.0A output
- One USB cable, standard-A plug to micro-B plug
- One Ethernet cable
- One daughter card (HW-RFMC-XM500)
- SMA cables
- Class-10 Micro SD card
- Cables and Filters Supplied with the board

It has to be noted that the most important element of ZCU111 is the connection between the data converters and the outside world and this is possible through two RFMC connectors, one for RF outputs, one for RF inputs. The HW-RFMC-XM500 is a balun board which connects the two interfaces and allows to pass from a balanced configuration to unbalanced one and vice versa. This external component allows to control up to 4 channels, 2 at Low Frequency and 2 at Radio Frequency. The system under investigation is shown in the following figure:

Figure 4.2.2.1 – Set up of the loopback test

After correctly set up the connection between the two boards and the PC host (ethernet connection) a two-tone involving the RF channels loopback analysis can be performed.

The DACs used for this are the DAC0 and DAC1 in tile 1. First, a correct set up of the DACs involved is necessary to generate the correct signals.

- The sampling frequency of the DAC is set up at 6389.76 MHz
- A complex signal has to be generated, so in the cross bar is selected "I & Q" mode
- An interpolation x8 is set up, so the data rate in the PL will be 798.72 MHz
- The complex mixer is set up on "fine" with frequency 1500 MHz

The ADCs used are the ADC01 and ADC23 in tile 1. A correct set up of the ADCs involved is necessary to correctly receive the signals:

- The sampling frequency of DACs is set up at 3194.88 MHz
- A complex signal has to be received, so in the crossbar is selected "I & Q" mode
- A decimation x4 is set up, in order to find the same data rate as before
- The complex mixer is set up on "fine" with frequency -1200 MHz

In the generation tab, available for each DAC, two tones with center frequencies 150 MHz and 200 MHz are generated. As mentioned in the previous section the generation of complex signals allows the use of one side-band transmission. In this case the two generated complex tones consider the negative contributions, as showed in the following figure (only related to carrier frequency (CF) = 150 MHz):
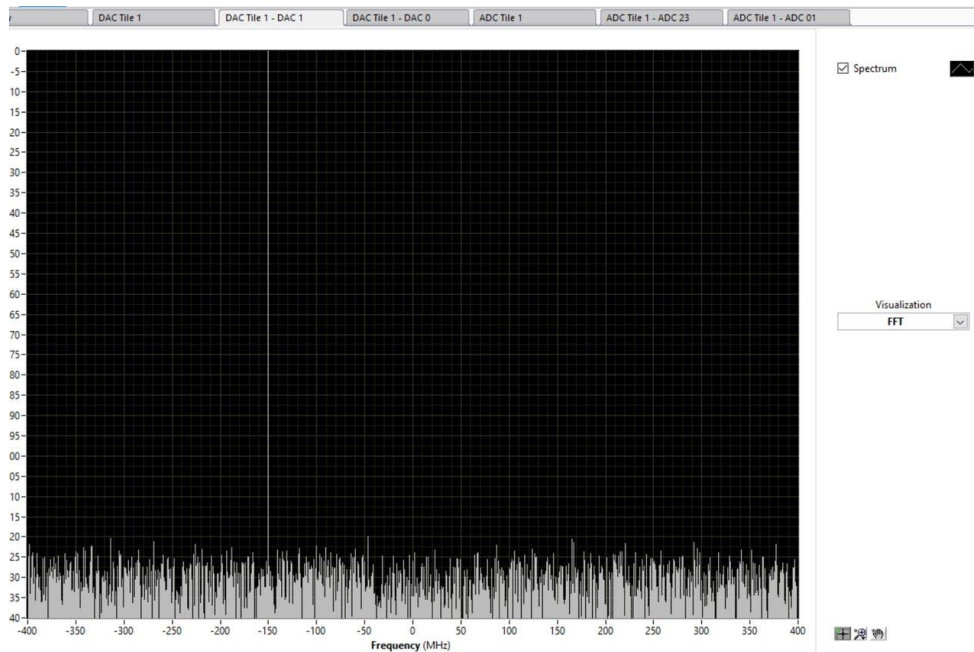

Figure 4.2.2.2 – DAC generation tab window

Therefore, considering the CF = 150 MHz and recalling what explained before we have:

- In the digital up converter

$$x_{RF}(t) = x_{bb}(t) * x_{CF}(t) = \cos(2\pi(f_{BB} + f_{CF})t)$$

  The product corresponds to a tone at 1550 – 150 = 1350 MHz

- In the digital down converter

$$x_{BB}(t) = x_{RF}(t) * x_{CF}(t) = \cos(2\pi(f_{RF} + f_{CF})t)$$

  The product corresponds to a tone at 1350 -1200 = 150 MHz

The same analysis can be done with CF = 200 MHz considering again the negative spectrum, the results of the product after the reception will give a tone at 100 MHz.

In the acquisition tab, available for each DAC, it is possible to visualize the received signals at baseband after the digital down conversion. The results are shown in the following figures:
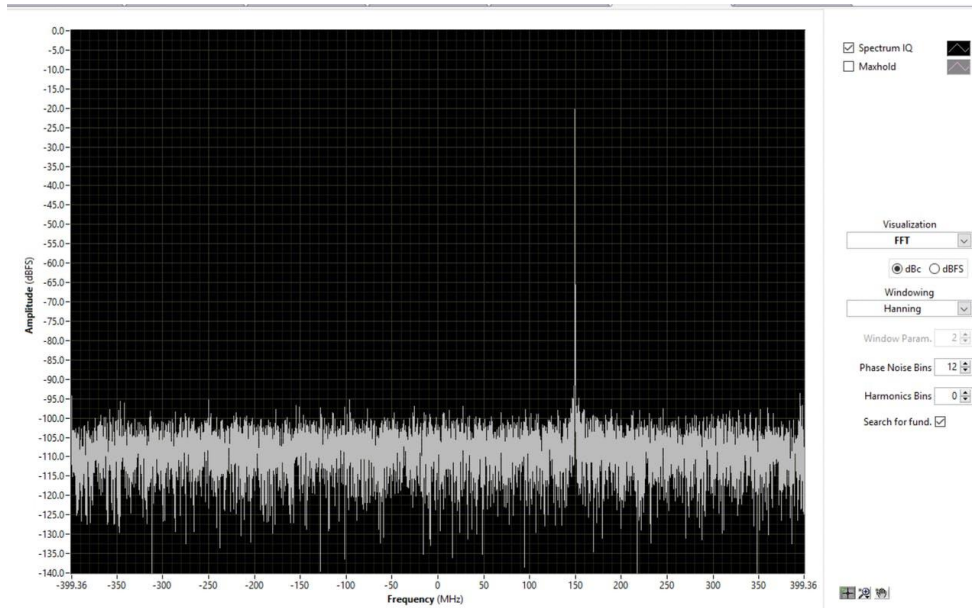
51

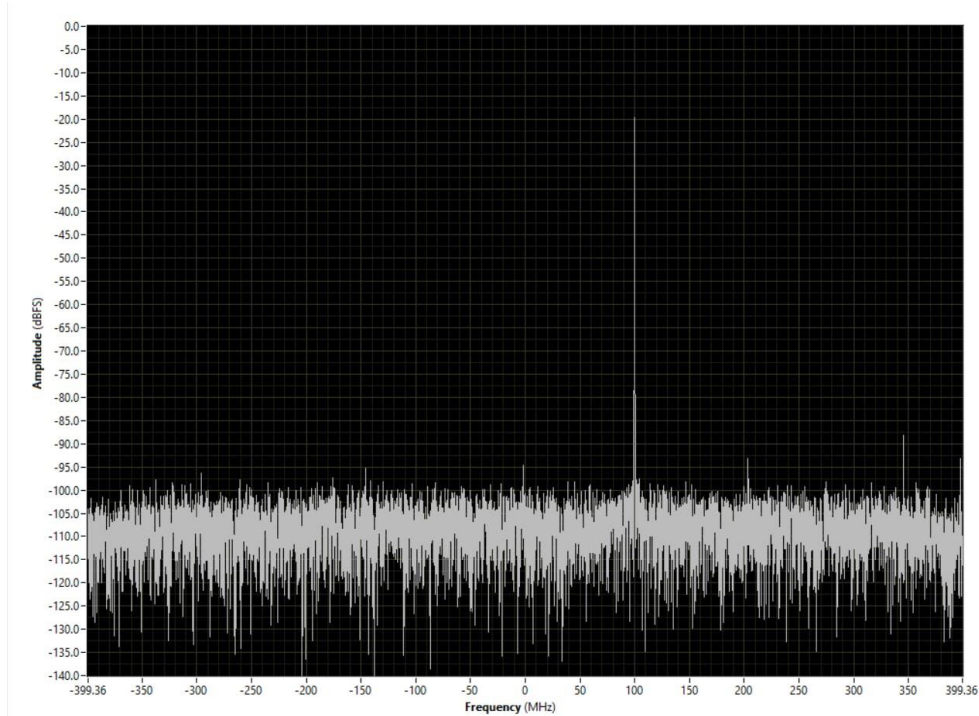*Figure 4.2.2.3 – ADC acquisition tab window for the CF=150 MHz case*

Figure 4.2.2.4 – ADC acquisition tab window for the CF=200 MHz case

It is worth noticing that the received signals result attenuated about 20 dB due to cables and filters.

4.2.3. RF CHARACTERIZATION OF THE ZYNQ ULTRASCLE+ RFSoC ZCU111

This section will deal with the RF characterization of the output signals generated by the Zynq Ultrascale+ RFSoC ZCU111. The simulation views provided by the tools shown in the previous section is not enough for a complete analysis, especially if it is needed to check the spectral purity offered by the system. For this purpose, a spectrum analyzer is needed and it will be connected to the output of the system in order to check its linear behaviour.

The equipment for the experiment is provided:

- ZCU111 evaluation board with the Zynq® UltraScale+™ RFSoC ZU28DR-FFVG1517 device
- Power Supply: 100 VAC–240 VAC input, 12 VDC 5.0A output
- One USB cable, standard-A plug to micro-B plug
- One Ethernet cable
- One daughter card (HW-RFMC-XM500)
- SMA cables
- Class-10 Micro SD card
- SMA CABLE (1)
- Spectrum analyzer

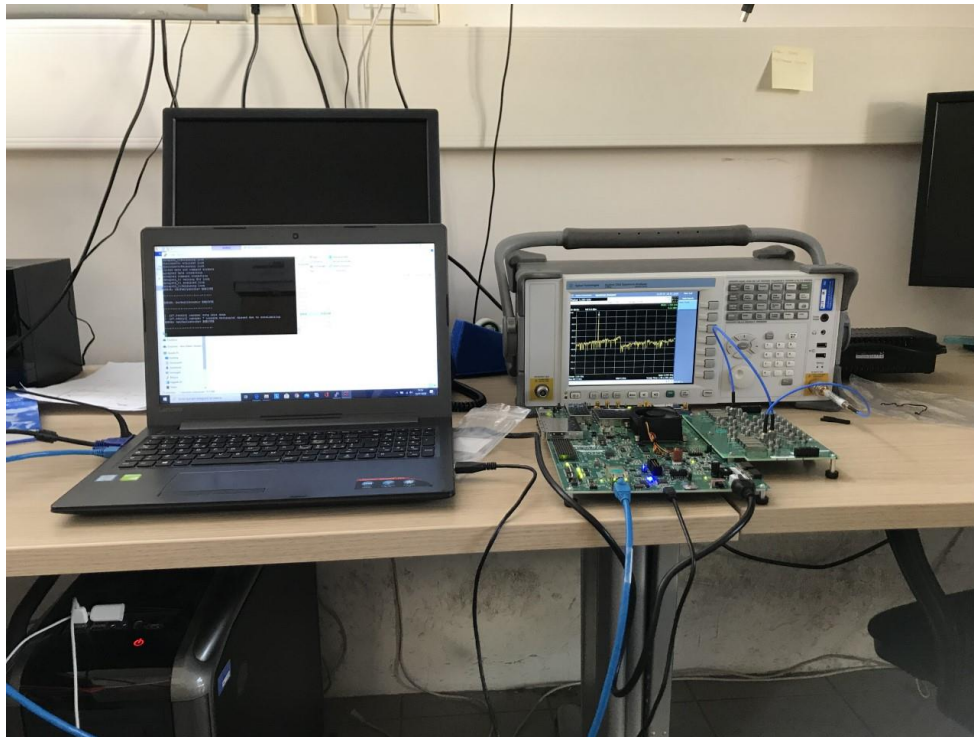The set up is shown in the following figure:

Figure 4.2.3.1 – Set up for RF characterization

As it is possible to notice the RF output of DAC1 in tile 1 provided by the HW-RFMC-XM500 external board is routed directly to the spectrum analyzer that will provide the spectrum properties until 6 GHz, while the DAC0 in tile 1 and ADC0 ain tile 1 are connected for emulating the loopback test.

For this RF characterization only one channel will be involved, i.e. DAC1 of the tile 1. The test will be split in two parts: the first one will have the aim to validate what was found in the loopback test, looking at the RF spectrum generating a complex tone, the second one will consider the analysis of one real tone test and two tone test.

COMPLEX TONE ANALYSIS

Therefore in the first analysis the same characteristic of the loopback test will be simulated going to visualize the output properties offered by spectrum analyzer.

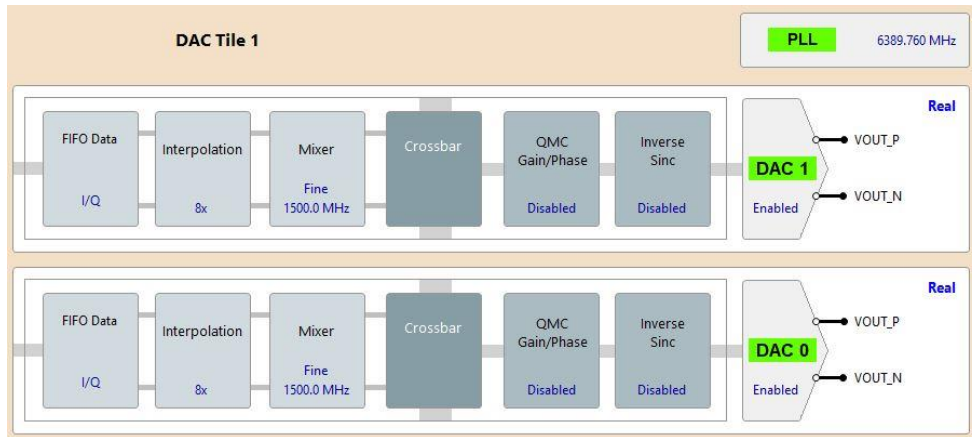The parameters of the DAC1 (RF test) and DAC0 (loopback test) are provided:

Figure 4.2.3.2 – DAC configuration in RFDC evaluation tool

Remembering what explained in the previous sections, a complex tone represented here will present a negative component at -150 MHz that will be mixed with a NCO at 1500 MHz. The results of the mixing will produce a lines at 1350 MHz. It has to be denoted that when the pass from analytical signal to real signal, the spectrum will present positive and negative component. The repetition in the digital domain of the negative component will generate at RF a component symmetric to the positive one respect to Fs/2. The following figure is introduce to explain the phenomena:
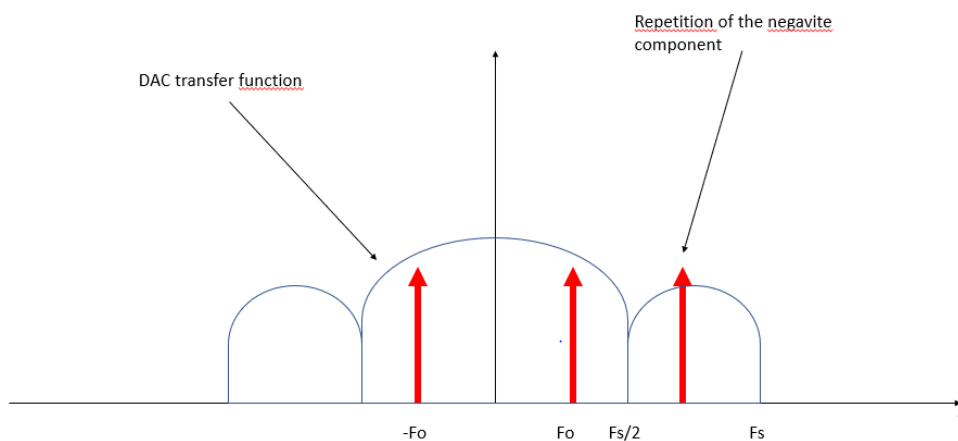

Figure 4.2.3.3 – Sketch of the output spectrum

Therefore, what it is expected will be a tone at 1350 MHz and a tone symmetric to this with respect to Fs/2, i.e., at 5040 MHz, that will be the negative image repetition, attenuated by the DAC response. The results are provided in the following figure:
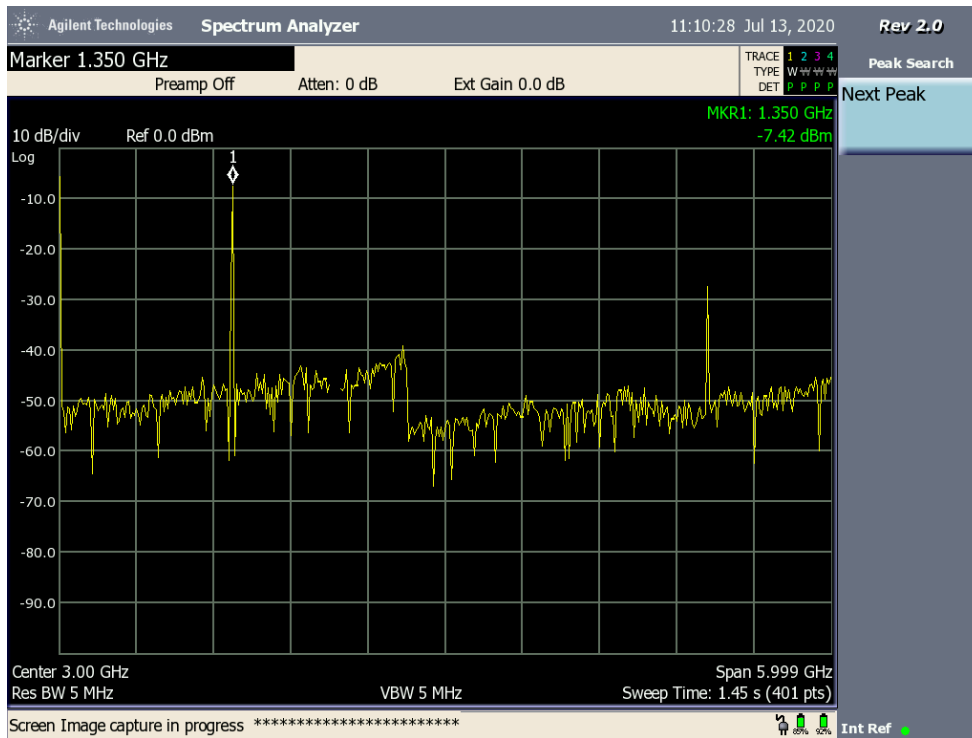
54

Figure 4.2.3.4 – Complex tone analysis at RF, output spectrum

In order to eliminate this component a low pass filter with passband 0 -2500 MHz is introduced. The effect of this filter can be associated to the selective behaviour of the monopoles used in the array that will cancel everything that is out of antennas operating band. The result is provided in the following figure:
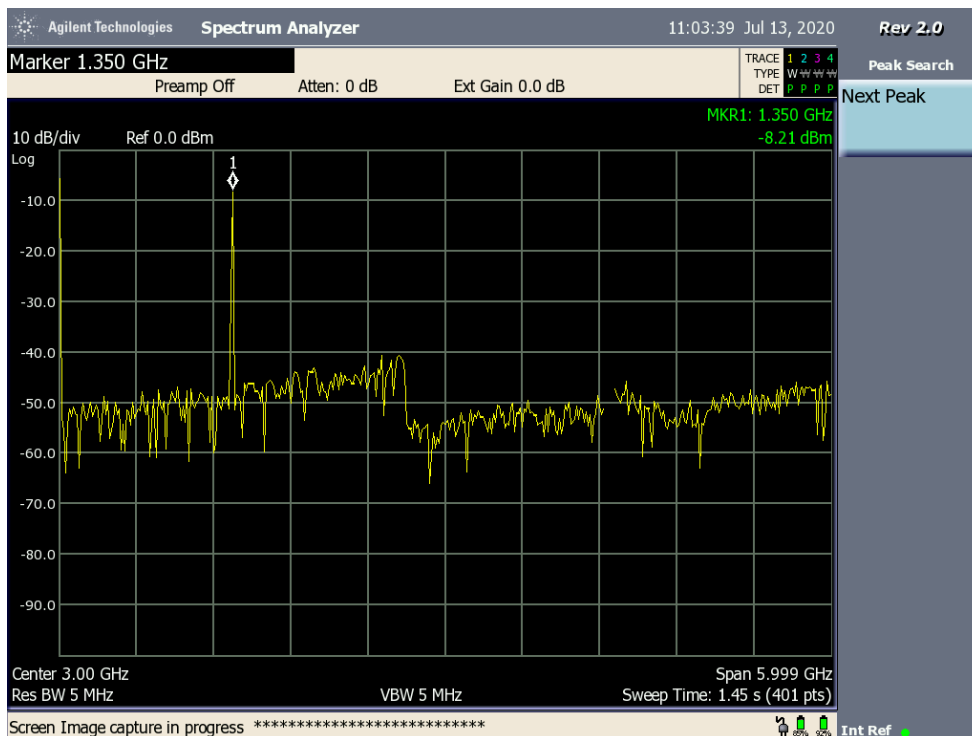

Figure 1.2.3.5 – Complex tone analysis at RF, output spectrum with filtering

After this evaluation, looking at the spectral purity, it can be denoted the excellent RF performance offered by the system, in which the harmonic products are negligible. This highlights the optimum spectral purity offered by the system.

ONE REAL TONE ANALYSIS

For the real tone analysis the set-up of the DAC1 is provided in the following figure:
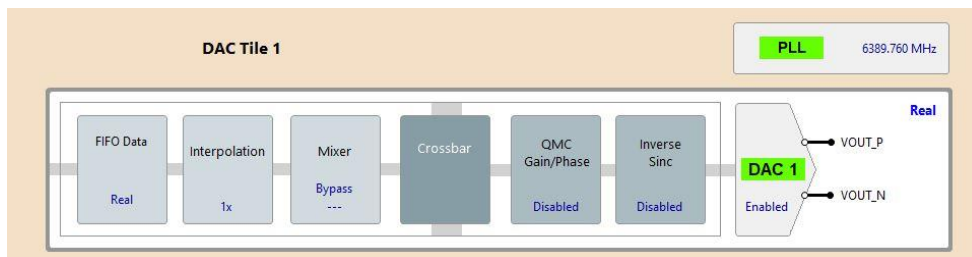

Figure 4.2.3.6 – set up of the DAC for RF characterization, real tone case

In the generation tab a stimulus of a real signal with center frequency CF = 2.4 GHz is provided as shown in the following figure:
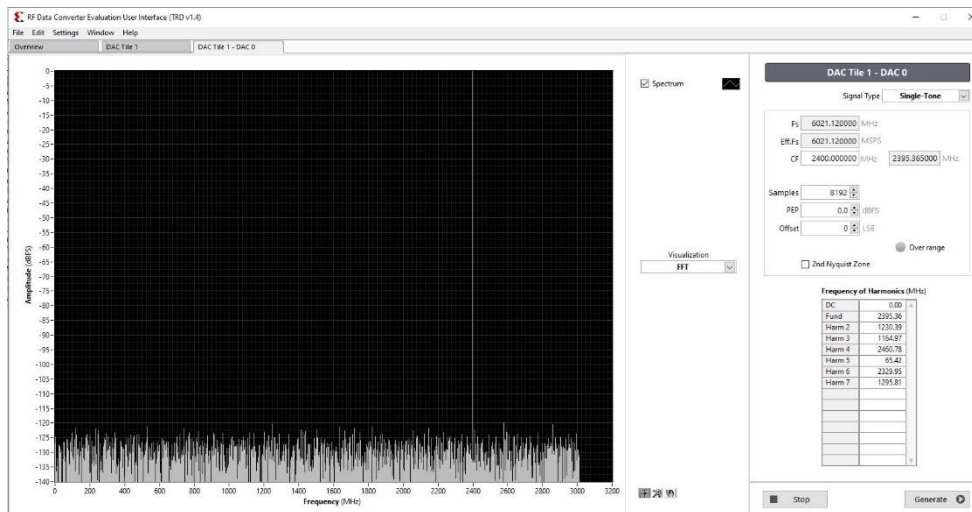

Figure 4.2.3.7 – DAC generation tab window

Before observing and commenting the results provided by the spectrum analyzer the same considerations done before, regarding the negative and positive component of a real signal, have to be taken into account. Therefore, what is expected is to visualize a tone at the desired frequency 2.4 GHz and an image at around 3.990 GHz. The "undesired component" is given by the fact that, before the DAC, we have a digital signal whose spectrum consists of the periodic frequency repetition with period Fs of the corresponding analog signal. Since one tone is generated, in the digital domain we have the two components at 2.4 GHz and – 2.4 GHz repeated every Fs, therefore the component around 3.9 GHz is the repetition of negative component after one sampling period Fs and that the DAC cannot eliminate but only attenuate, given the nature of its

transfer function. Therefore, in the second Nyquist zone (3GHz-6GHz) the presence of this additional contribution is perfectly reasonable.

The results extracted with the spectrum analyzer are provided in the following figure:
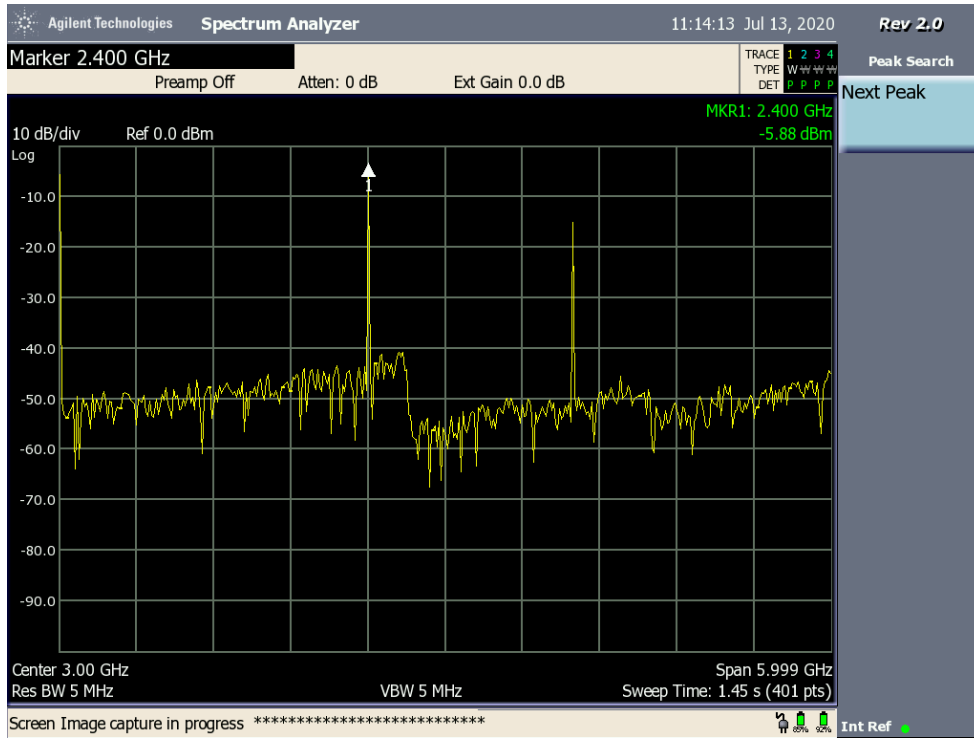

Figure 4.2.3.8 – Spectrum analyzer one real tone output spectrum, desired component
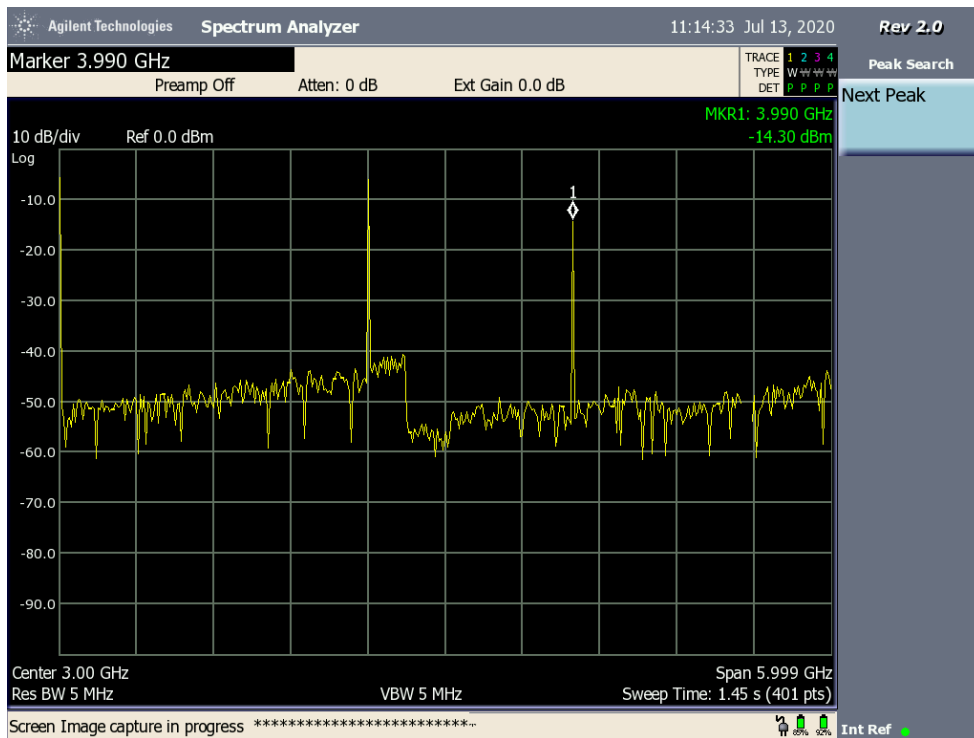

Figure 4.2.3.9 – Spectrum analyzer one real tone output spectrum, undesired component

As expected in the output spectrum both the useful tone at 2.4 GHz and the undesired image symmetric to Fs / 2 have been found. As done before, a low pass filter mimicking the effect of the monopoles in the array is inserted, thus eliminating the undesired line. The output properties with filtering is proposed in the following figure:

Figure 4.2.3.10 - Spectrum analyzer one real tone output spectrum with filtering

For what concern the spectral purity, the figures show again the high linearity of the system in the one tone case: in fact, the superior harmonic products are practically negligible.

TWO REAL TONES ANALYSIS

As second test a two tones analysis is provided. The set up for the configuration of the DAC0 in tile 1 is not modified, instead in the generation tab a two-tone stimulus is needed. The two tones are generated at 2.35 GHz and 2.45 GHz, respectively. The same consideration about the presence of the image has to be taken into account.

The results extracted with the spectrum analyzer are provided in the following figure:
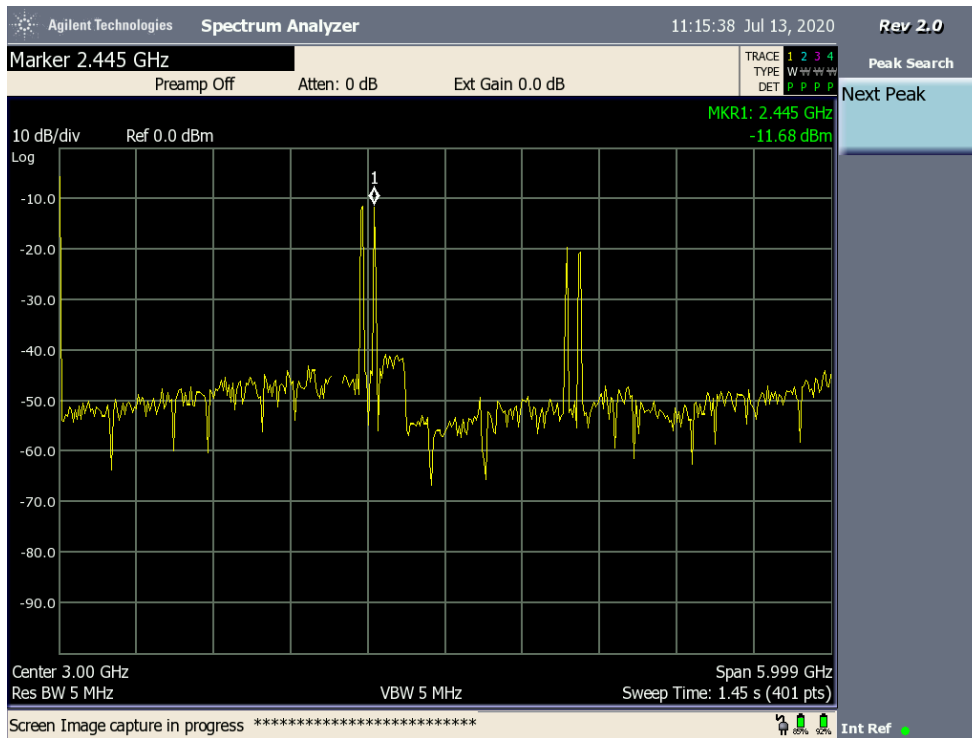
Figure 4.2.3.11 - Spectrum analyzer two real tones output spectrum

As expected, the desired components at 2.4 GHz and 2.45 GHz and the undesired images as before, symmetrical respect to Fs/2 have been found. Also in this case, with use of proper filtering, the undesired image can be eliminated, as shown in the following figure:
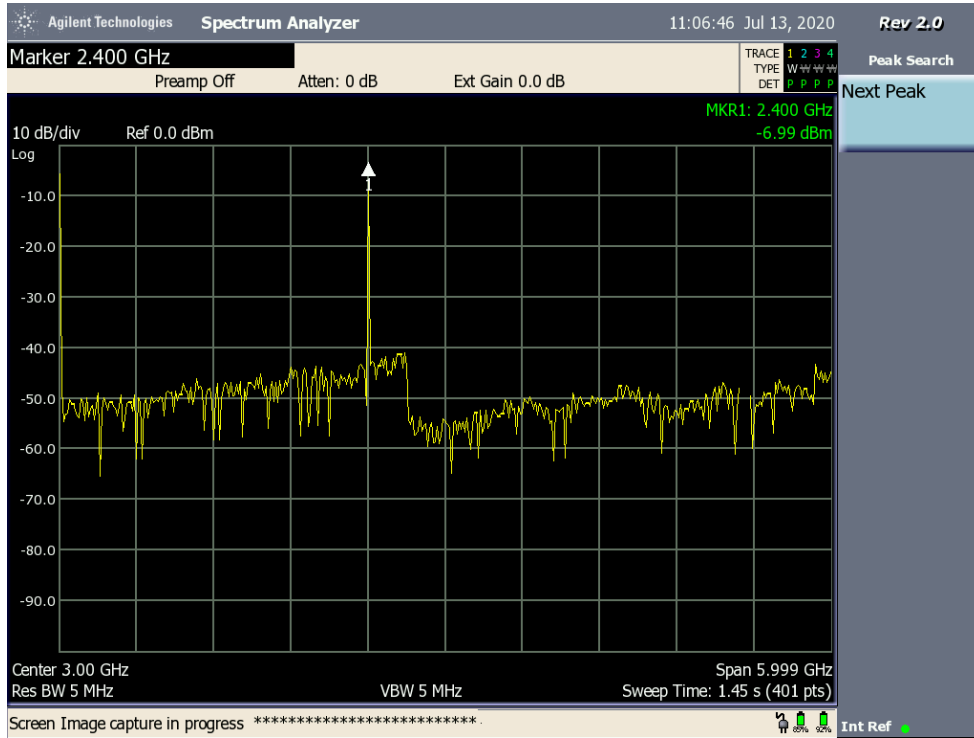

Figure 4.2.3.12 - Spectrum analyzer two real tones output spectrum with filtering

For what concern the spectral purity, the figures show again the great linearity of the entire system because of the absence of the higher-order intermodulation products.

59

The analyses reported in this section have confirmed the excellent linearity of the board and the consequent high spectral purity.

5. FINAL LAYOUT AND CONCLUSIONS

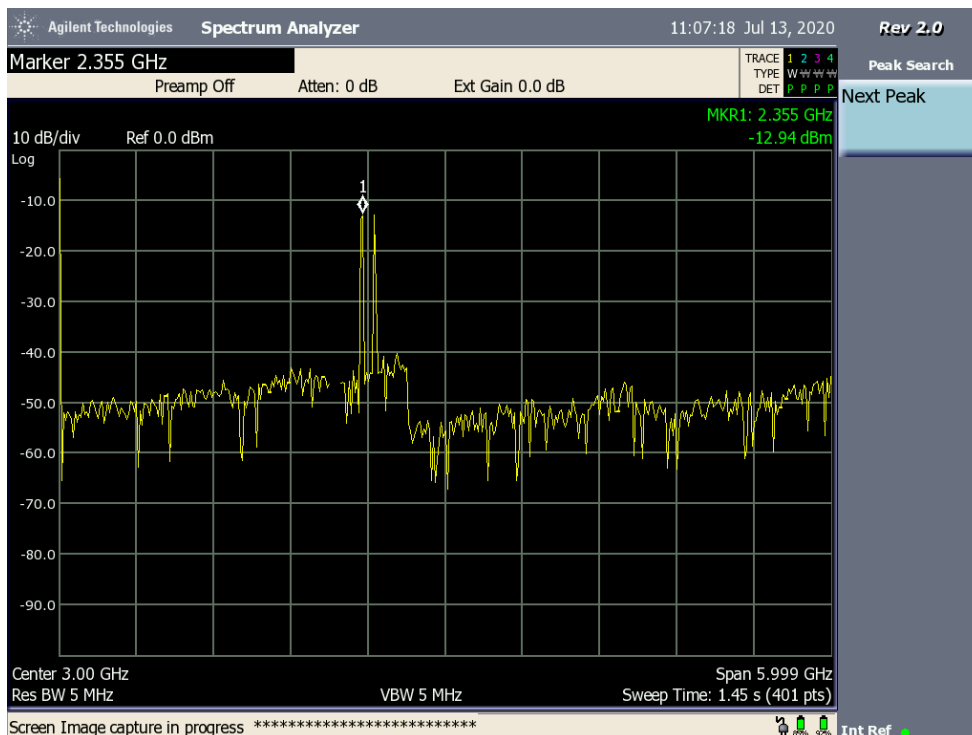## 5.1. PRACTICAL IMPLEMENTATION OF THE logfreqFDA SYSTEM

This chapter will deal with the presentation of final layout for creating a first prototype of a logfreqFDA system. The idea is to use the SDR platform Zynq Ultrasclae+ RFSoC ZCU111 in order to control all 8 RF channels [5]. The output will be extracted with an external board called AES-LPA-502-G that allows to manage all 8 differential RF outputs. A detailed presentation of this external board will be provided later in this chapter. Finally, with 16 SMA cables (2 per each differential output) the signals will be routed to the FDA array explained in the chapter 2 composed by 8 monopoles. It has to be noted that 8 SMD baluns are needed in order to pass from a balanced configuration (differential outputs) to unbalanced configuration (antenna microstrip input lines). The SMD baluns will be presented later in this section.

The block scheme of the entire prototype is provided:
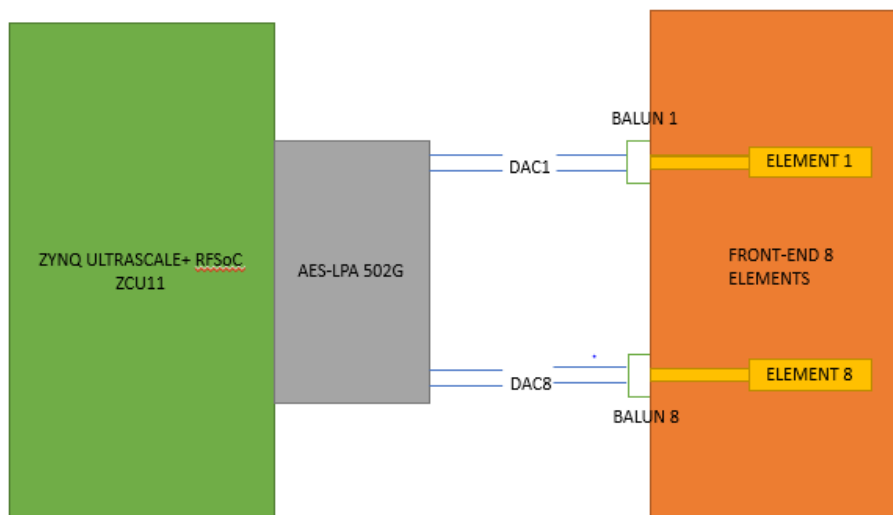

Figure 5.1.1 – Block scheme of the prototype

The external board AES-LPA-502-G is connected through the RFMC connectors as HW-RFMC-XM500 in the previous characterization. A description of the used components follows.
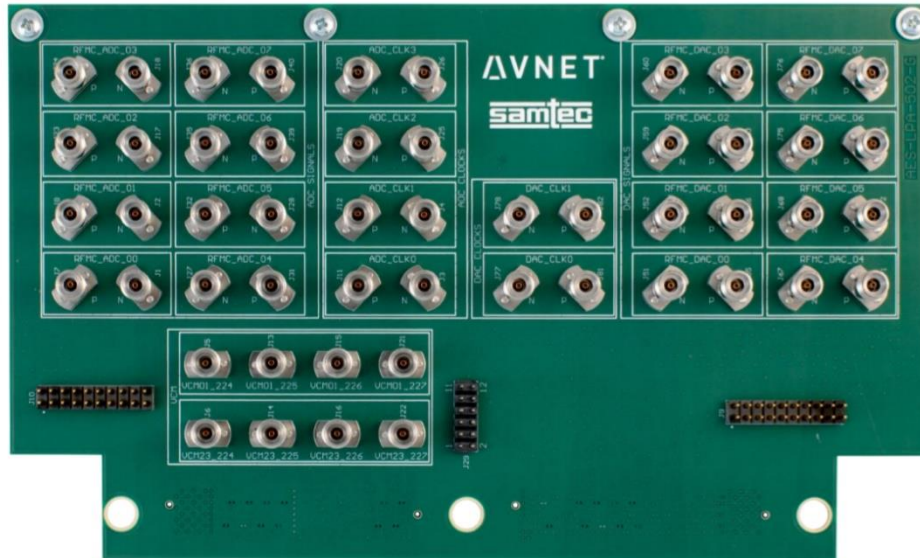
AES-LPA-502-G

Figure 5.1.2 – AES-LPA-502G

The AES-LPA-502-G is a daughter card for the Xilinx Zynq® UltraScale+™ RFSoC ZCU111 Evaluation Kit. A completely passive board with no filtering or baluns, it is intended as a break-out for RF-ADCs and RFDACS of the Zynq UltraScale+ RFSoC device to external test equipment. AES-LPA-502-G provides access to the 8 channels of RF-ADC and RF-DACS of the Zynq UltraScale+ RFSoC device on ZCU111 through fully differential, 50-Ohm length-matched traces via two Samtec LPAM (8x40) connectors on the bottom of the card. The key features are listed below:

- J333 LPAM-40-01.0-S-08-2-K-TR – ADC
- J888 LPAM-40-01.0-S-08-2-K-TR – DAC
- Eight DACs and eight ADCs routed to RF connectors
- Four pairs external input clocks for ADCs routed to RF connectors
- Two pair external input clocks for DACs routed to RF connectors
- RFSoC bank 224-227 VCM nets routed to RF connectors
- Access RFMC digital I/O (40 bits) at standard headers
- Access to RFMC I2C, 1.8V, 3.3V, 12.0V and DAC_AVTT at standard headers
- Leverages Samtec RSP-208784-01 screw-mount, straight SMA plug

The connection between the AES-LPA-502G and the Zynq Ultrasclae+ RFSoC ZCU111 is reported in the following figure:
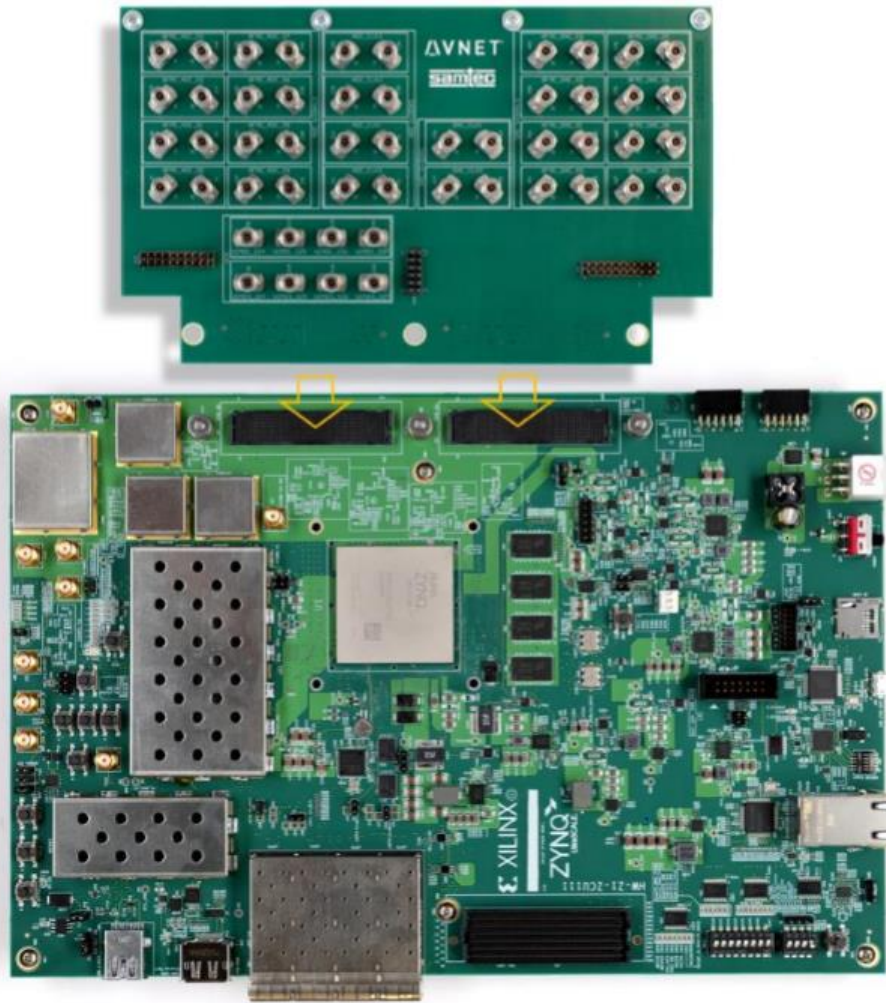
Figure 5.1.3 – Connection between AES-LPA-502G and Zynq Ultrascale+ RFSoC ZCU111

RF CABLES AND SMD BALUNS

The connection between the AES-LPA-502-G and the front-end is provided through RF cables with SMA-type terminations. Since the outputs provided by the external board are differential, baluns are needed to be installed in the front-end before the array. Since the differential outputs provide an output impedance of 100 Ohm, with each via offering 50 Ohm, the requested impedance of the cables has to be 50 Ohm, hence the balancing of impedance offered by the baluns has to provide a passage from balanced 100 Ohm to unbalanced 50 Ohm. Important parameter is also the length of cables that should be at least 60 cm, in order to allow the connection with all the array elements placed l/2 apart from each other.

Several phenomena have to be taken into account as AC and DC coupling. Most of all it is strongly recommended to read the technical paper UltraScale Architecture PCB Design User Guide avaible on Xilinx site. [

Hence for the final layout needs for 8 baluns and 16 RF cables. Examples of both are given in the following figures:

Figure 5.1.4 - Example of RF coaxial cable with SMA connectors, Coaxial cable Cinch Connectors RG-316DS, L. 610mm, 50 Ω

The features of the RF coaxial cable have to be: i) 50 Ohm as characteristic impedance, ii) around 60 cm of length, iii) male-type SMA terminations, and iv) an operating bandwidth that comprehends the desired set of frequencies (placed around 2.45 GHz).

The SMD baluns will be mounted on the PCB of the 8-mopoles planar array. An example of commercially available balun is shown in the following figure:
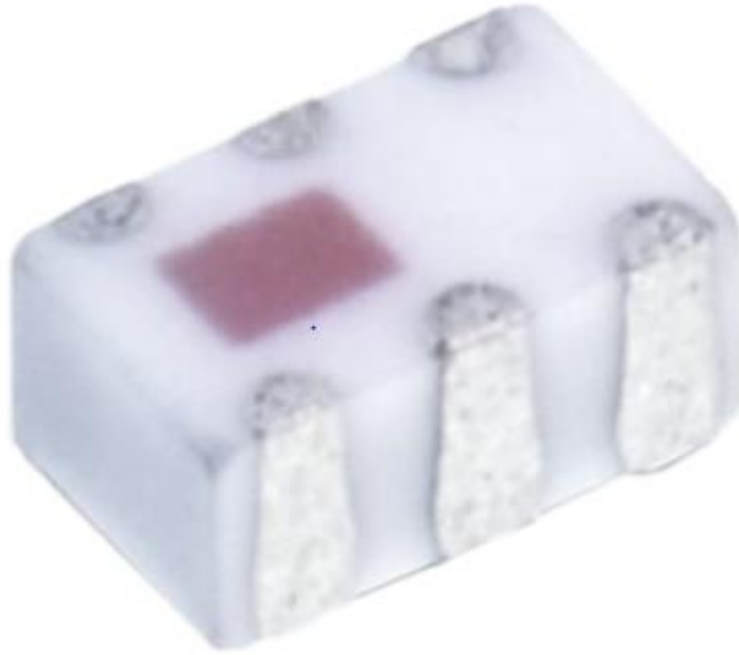
Figure 5.1.5 – Example of SMD Balun, Chip Balun Wurth Elektronik, Zsbilanc. 50Ω, Zbilanc. 100Ω, SMD

The characteristics that the balun should have for the project under investigation are listed in the following:

Unbalanced configuration	50Ω
Balanced configuration	100Ω
Maximum insertion loss	1dB
Mounting type	Superficial
Dimension	2 x 1.25 x 0.85 mm3
Maximum Frequency	2.5GHz
Minimum Frequency	2.4GHz
Maximum operating temperature	+85°C
Minimum operating temperature	-40°C

5.2. CONCLUSION

An investigation on the FDA systems has been developed in order to exploit them in WPT scenarios for the maximization of the RF-to-RF efficiency. The standard FDA, the logdistFDA and the logfreqFDA have been considered during this investigation and an analytical evaluation of their properties has been provided in chapter 2, reaching the conclusion that the logfreqFDA offers the best performance in terms of focus of the power in a restricted area, despite the time-dependent behaviour. In chapter 3 the design of the single monopole antenna and the 8-elements array has been provided and their performance have been extracted through electromagnetic simulations with CST. The simulation provided with CST have been used in the second simulation phase, using the Harmonic Balance method to investigate the complete and realistic logfreqFDA system behaviour taking into account the electromagnetic coupling between the elements and the actual nonlinear regime taking place at circuit level. The obtained results have confirmed the good performance offered by the system under investigation. For the first time an HB simulation has been provided for this type of radiating structure, in particular the time-dependent behaviour has been simulated confirming the results provided by the numerical simulation in the previous chapter. Again the quality of the system has been highlighted. It is worth noticing that the results of this chapter will be published on [5] and represent the first trial in the literature to provide an accurate description of the complex radiating mechanism of FDA systems, also from the time-dependency point of view.

In chapter 4 for the first time it has been introduced a new method for the control of the excitation signals of the system under investigation. The SDR technology has been the choice for this delicate task and the Zynq Ultrascale+ ZCU111 evaluation kit has been adopted. The passage from analog to digital domain has been provided in the first part. In the second part the architecture of the board under investigation has been provided, with particular emphasis on the RF Data Converter subsystem and its relative tool, able to allow to the user to completely define the RF signal chain of the DDC and DUC subsystem. A characterization of the board has been provided with two types of experiments: the first one is a simulation of a loopback test able to show the working principle of the RF Data Converter Evaluation Tool in which complex tones using two channels have been used. The second is an experimental test able to show the RF characteristic of the outputs in terms of spectral purity exciting one channel of the system with a real tone. The results of both the tests have highlighted the optimum performance provided by the Zynq Ultrasclae+ ZCU111 board, reaching to the conclusion that the choice of using an SDR platform for controlling FDA systems is the only one that can be quite easily implemented. For the signal set generation needed in the radiating system under construction it can be said that a knowledge of program languages for interfacing embedded systems is not necessary. In fact, through MATLAB&SIMULINK the signals of interest can be generated and uploaded on the PL system of the board with special transducers, using the same graphic tool. This method will result very helpful since, as has been highlighted before, the signals have to be modified in order to counterbalance the effect of the time- dependent behaviour, turning on and turning off the elements in the proper instants.

Finally, a complete layout description of the entire system has been provided, looking at the practical implementation of the logfreqFDA system. In particular new components have been proposed: the AES-LPA-502G, able to provide the access to all the 8 RF channels in fully differential way, RF cables and SMD baluns able to provide the connection between the SDR platform and the front end. The steps described in this chapter have been described also in [6] and will be published soon: also in this case, the adopted architecture represents the first attempt in the literature to realize an FDA. A deeper investigation in the realization of the architecture here proposed has to be performed in the near future in order to counterbalance possible undesired effects. Most of all, a delicate measure campaign will be carried out after a first prototype will be available.

However, there is space for further investigations. The strength of the FDA system has been highlighted and for the first time a practical implementation example has been proposed considering the SDR platform for

supporting the generation and control of the signal. But improvements with the aim of deeply understand the use of ZCU111 board have to be done. The interface between MATLAB&SIMULINK and the board has to be investigated further in order to correctly set up the sequences needed for counterbalance the time - dependent effect. Tests with the AES-LPA-502G have to be performed in order to study the RF characteristics offered by this differential card. Finally, as already said, the 8-monopole FDA has to be built for practical tests in a real scenario.

Moreover, the recent literature offers new excitation strategies that have to be first simulated to verify their effectiveness, then implemented on the SDR to practically test them. One configuration able to improve the performance of the logfreqFDA can be exploited, by following the convex multilog FDA with multicarrier transmission proposed in [9] in order to obtain a Dot-Shaped Range-Angle Beampattern, by working on the complex weights and transmission signals. The beampattern would result as in the following figure:
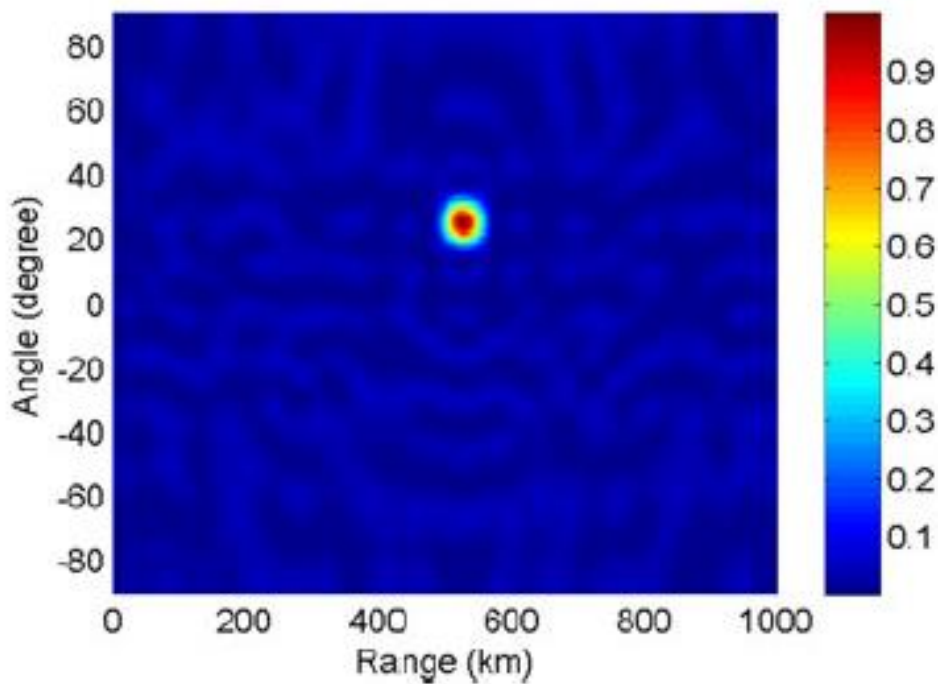

Figure 5.2.1 – Convex multi-log FDA beampattern, t = 0 s, [5]

Another interesting example should be the design of Frequency Diverse Array Antenna using Time-Modulated Optimized Frequency Offset to obtain Time-Invariant Spatial Fine Focusing Beampattern [10] according to which, by working on the signal frequencies time distribution, a time-invariant beampattern can be obtained. This represents an additional (with respect to the one presented in this thesis work) approach to counterbalance the time-dependent behaviour. The results could be:
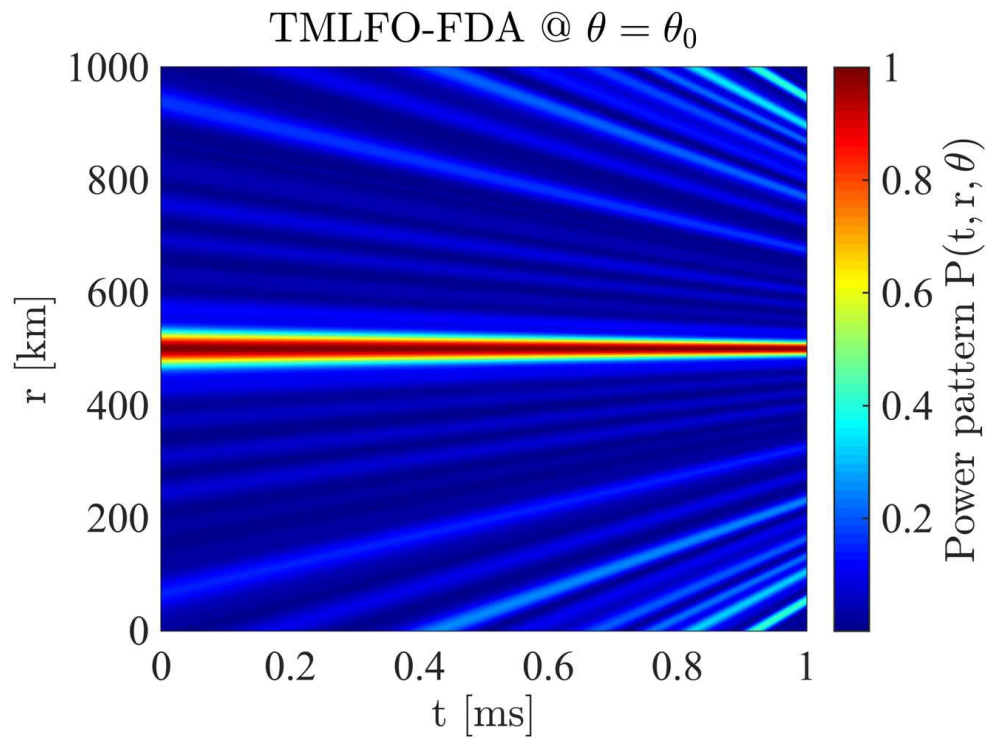
Figure 5.2.2 – beampattern of TMLFO-FDA time behaviour, [8]

The figure 5.2.2 represents the time behaviour of the Time-Modulated Logarithmic Frequency Offset

Finally, even the cost of the project is an important aspect to be taken into account. This is dominated by the cost of the ZCU111 and the relative components as AES-LPA-502G external board. A cheaper solution will be searched in the near future. However the work developed during this thesis is a first proof-of-concept of the possible realization of very promising radiating systems for WPT scenarios.

6. BIBLIOGRAPHY

1. https://en.wikipedia.org/wiki/Wireless_power_transfer

2. "Antennas for Wireless Systems" notes of the lectures of the course of A.A. 2018-19

3. "Technologies and Applications for Wireless Power Transfer" notes of the lectures of the course of A.A. 2019-20

4. "Energy Focusing Through Layout-Based Frequency-Diverse Arrays", D. Masotti, M. Shanawani, A. Costanzo,

5. "Focusing RF-on demand by Logarithmic Frequency Diverse Array", E. Fazzini, D. Masotti, M. Shanawani, A. Costanzo, accepted at WPTC 2020

6. "A Logarithmic Frequency-Diverse Array System for Precise Wireless Power Transfer", E. Fazzini, D. Masotti, M. Shanawani, A. Costanzo, accepted at EUMW 2020

7. W. Wang, H. C. So and A. Farina, "An Overview on Time/FrequencyModulated Array Processing," in *IEEE Journal of Selected Topics in Signal Processing*, vol. 11, no. 2, pp. 228-246, March 2017.

8. "W. Khan, I. M. Qureshi, and S. Saeed, "Frequency diverse array radar with logarithmically increasing frequency offset," *IEEE AntennaWireless Propag. Lett.*, vol. 14, pp. 499–502, 2015.

9. H. Shao, J. Dai, J. Xiong, H. Chen and W. Wang, "Dot-Shaped Range-Angle Beampattern Synthesis for Frequency Diverse Array," in *IEEE Antennas and Wireless Propagation Letters*, vol. 15, pp. 1703-1706, 2016.

10. A. Yao, W. Wu and D. Fang, "Frequency Diverse Array Antenna Using Time-Modulated Optimized Frequency Offset to Obtain Time-Invariant Spatial Fine Focusing Beampattern," in *IEEE Transactions on Antennas and Propagation*, vol. 64, no. 10, pp. 4434-4446, Oct. 2016

11. Y. Liao, W. Wang and H. Shao, "Symmetrical logarithmic frequency diverse array for target imaging," *2018 IEEE Radar Conference (RadarConf18)*, Oklahoma City, OK, 2018, pp. 0039-0042

12. "Frequency Diverse Array Beampattern Synthesis Using Symmetrical Logarithmic Frequency Offset for Target Indication" Yi Liao, Wen-Qin Wang and Zhi Zheng, *IEEE TRANSACTIONS ON ANTENNAS AND PROPAGATION,* vol. 67, NO.5, MAY 2019

13. Zynq UltraScale+ RFSoC RF Data Converter Evaluation Tool (ZCU111) *User Guide*

14. ZCU111 Evaluation Board *User Guide*

15. Vivado Design Suite User Guide *Designing IP Subsystems Using IP Integrator*

16. Vivado Design Suite User Guide *Getting Started*

17. Vivado Design Suite User Guide: Logic Simulation

18. Vivado Design SuiteUser Guide *Designing with IP*

19. Zynq UltraScale+ RFSoC   RF Data Converter 2.1 *LogiCORE IP Product Guide*

20. Zynq UltraScale+ RFSoC Data Sheet: DC and AC Switching Characteristics

21. RFSoC UltraScale+ Evaluation Board HW-Z1-ZCU111